Signatures of quantum chaos in rare-earth elements: II. Characterization of the energy eigenvalues and dipole moments of Ce I and Pr I

To cite this article: A Cummings *et al* 2001 *J. Phys. B: At. Mol. Opt. Phys.* **34** 3447

View the article online for updates and enhancements.

Related content

- Signatures of quantum chaosin rare earth elements: I
  A Cummings, G O'Sullivan and D M Heffernan

- Characterization of the structure and eigenvalue spectra of the compound states of Sm IX
  D Kilbane, A Cummings, D M Heffernan et al.

- 4f collapse, level density inflation and the emergenceof `compound-like' atomic states in rare earthions
  D Kilbane, A Cummings, C McGuinness et al.

Recent citations

- Ground-state configurations and theoretical soft-x-ray emission of highly charged actinide ions
  J. Sheil *et al*

- Characterization of the structure and eigenvalue spectra of the compound states of Sm IX
  D Kilbane *et al*

- Signatures of two-body random matrix ensembles in Sm I
  Dilip Angom and V. K. B. Kota

Signatures of quantum chaos in rare-earth elements: II. Characterization of the energy eigenvalues and dipole moments of Ce I and Pr I

A Cummings[1,2], **G O'Sullivan**[1] **and D M Heffernan**[2,3]

[1] Physics Department, University College Dublin, Dublin 4, Ireland
[2] Department of Mathematical Physics, National University of Ireland Maynooth, Maynooth, Co. Kildare, Ireland
[3] School of Theoretical Physics, Dublin Institute for Advanced Studies, Dublin 4, Ireland

Abstract
Using the relativistic configuration interaction Hartree–Fock method the energy eigenvalues and dipole moments of Ce I, $J = 4^{\pm}$ and Pr I, $J = 11/2^{\pm}$, both members of the rare earth sequence, are examined for the presence of signatures of quantum chaos, using the following spectral statistics: nearest neighbour spacing, covariance of adjacent spacings, spectral rigidity, correlation-hole method and $\chi^2(\nu)$ probability distribution.

1. Introduction

This is part II of a two-part study involved in investigating the signatures of quantum chaos in rare-earth elements. In part I [1] the characterization of the Hamiltonian matrices and coupling matrices of Ce I and Pr I was pursued and it was found that the distribution of the off-diagonal many-body matrix elements of the Hamiltonian of the configuration interaction Hartree–Fock (HFCI) method, in both the ls and jj coupling schemes, was close to exponential, as was found previously in [2]. The Hamiltonian does not contain any random elements and any possible 'chaoticity' arises as a result of mixing of the basis states. In the present case (part II) the characterization of the energy eigenvalues and dipole moments of Ce I and Pr I is examined. It is again important to stress that additional statistical tests are included that have not been used, to date, in previous studies [2] of the lanthanide elements.

Diagonalization of the Hamiltonian matrices of Ce I, $J = 4^{\pm}$ and Pr I, $J = 11/2^{\pm}$, of the previous study [1] results in a set of energy eigenvalues that can be statistically analysed [2–5]. From the Bohigas–Giannoni–Schmit conjecture [6]—'spectra of time-reversal invariant systems whose classical analogues are K systems show the same fluctuation properties as predicted by the GOE'—(the K systems mentioned in this conjecture are the most strongly mixing classical systems) the invariant measures of chaos associated with energy level statistics can indicate the presence or absence of 'quantum chaos'. These energy level statistics,

Table 1. (a) The even and odd configurations of Ce I and Pr I used as basis configurations for the Cowan suite of codes [8]. (b) Even and odd configurations of Ce I and Pr I [7].

(a)
Ce I $Z = 58$

Odd configurations	$4f5d6s^2$, $4f5d^26s$, $4f5d^3$, $4f^26s6p$, $4f5d6p^2$, $4f6s6p^2$, $4f^25d6p$
Even configurations	$4f6s5d6p$, $4f^26s^2$, $4f6s^26p$, $4f5d^26p$, $4f5d^26p$, $4f^26s5d$, $4f^25d^2$, $4f^26p^2$

Pr I $Z = 59$

Odd configurations	$4f^36s^2$, $4f^25d6s6p$, $4f^26s^26p$, $4f^35d6s$, $4f^25d^26p$, $4f^35d^2$, $4f^36p^2$
Even configurations	$4f^25d6s^2$, $4f^25d^26s$, $4f^36s6p$, $4f^35d6p$, $4f5d^26s6p$, $4f5d^36p$, $4f5d6s^26p$

(b)
Ce I

Odd configurations	$4f5d6s^2$, $4f5d^26s$, $4f5d^3$, $4f^26s6p$
Even configurations	$4f^26s^2$, $4f^25d6s$, $4f6s^26p$, $4f5d6s6p$ $4f5d^26p$, $4f^25d^2$

Pr I

Odd configurations	$4f^36s^2$, $4f^35d6s$, $4f^26s^26p$, $4f^25d6s6p$, $4f^25d^26p$
Even configurations	$4f^25d6s^2$, $4f^25d^26s$, $4f^36s6p$, $4f^35d6p$

namely the nearest neighbour spacing, covariance of adjacent spacings, spectral rigidity and correlation-hole method, thus form the results of sections 2–5 where the experimental energy eigenvalues [7] and the theoretical eigenvalues [8] for even and odd Ce I and Pr I are studied. In section 6, the line strengths are compared to a $\chi^2(\nu)$ probability distribution where $\nu = 1$ is indicative of classically chaotic behaviour, whereas $\nu = 0$ indicates classically regular behaviour.

2. Level statistics

Diagonalization of the Hamiltonian gives a set of energy eigenvalues that can be analysed and compared with the predictions of Random Matrix Theory (RMT), the density of states $\rho(E)$ being one of a number of possible spectral statistics. The configurations of table 1(a) were used as basis configurations, in the Cowan suite of codes [8], for Ce I (as used in the study of [1]) and Pr I. The configurations that give rise to the experimental (NIST) energy eigenvalues [7] are shown in table 1(b). The even and odd parity configurations of both species will henceforth be referred to as 'even Ce/Pr' and 'odd Ce/Pr' respectively. In a finite Hilbert space, $\rho(E)$ disappears at lower and upper boundaries of the spectrum, being maximum in the middle. This can be seen in figures 29 and 30 of the previous study [1], for Ce and Pr respectively. The behaviour of $\rho(E)$ can be compared with the Gaussian Orthogonal Ensemble (GOE) predictions [3], where the GOE predicts the Wigner semi-circle rule. The BRM theory predicts, both numerically and analytically [9–11], the semi-circle level density for a sufficiently broad band.

However, as has been pointed out in [1], the atomic Hamiltonian has no random elements. Also, due to the two-body character of interaction and exact conservation of
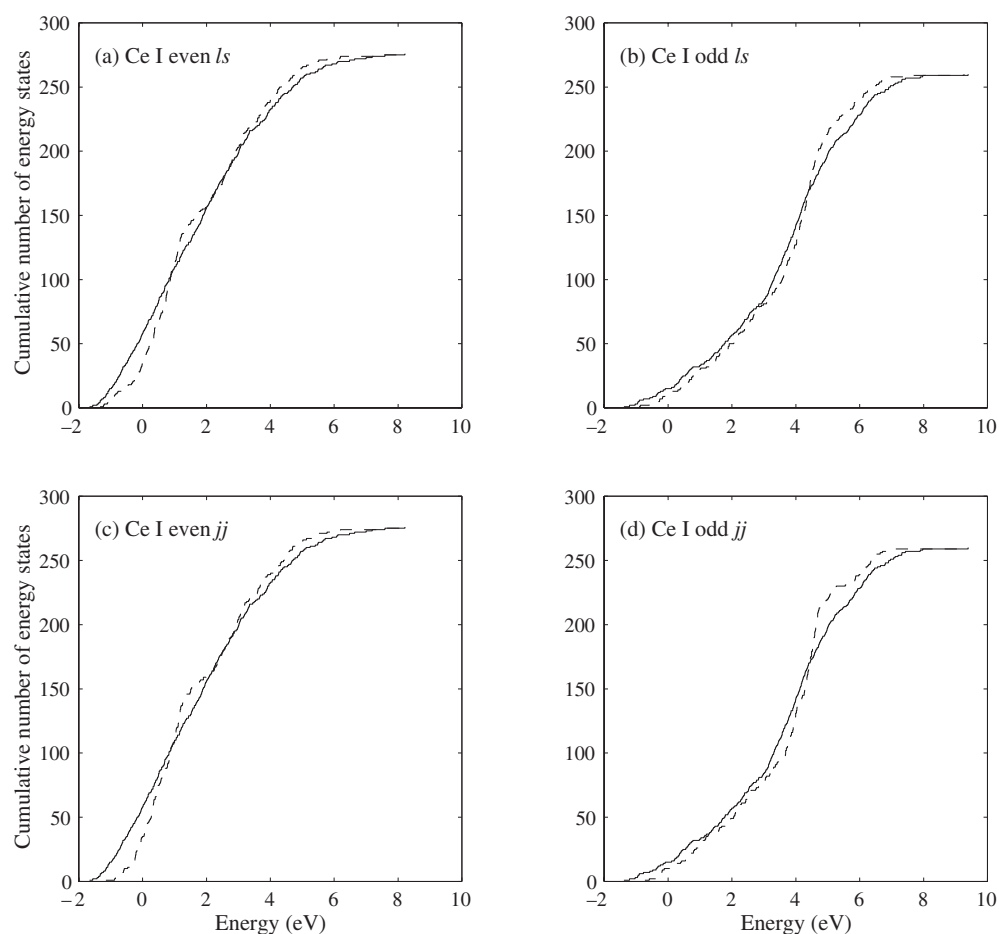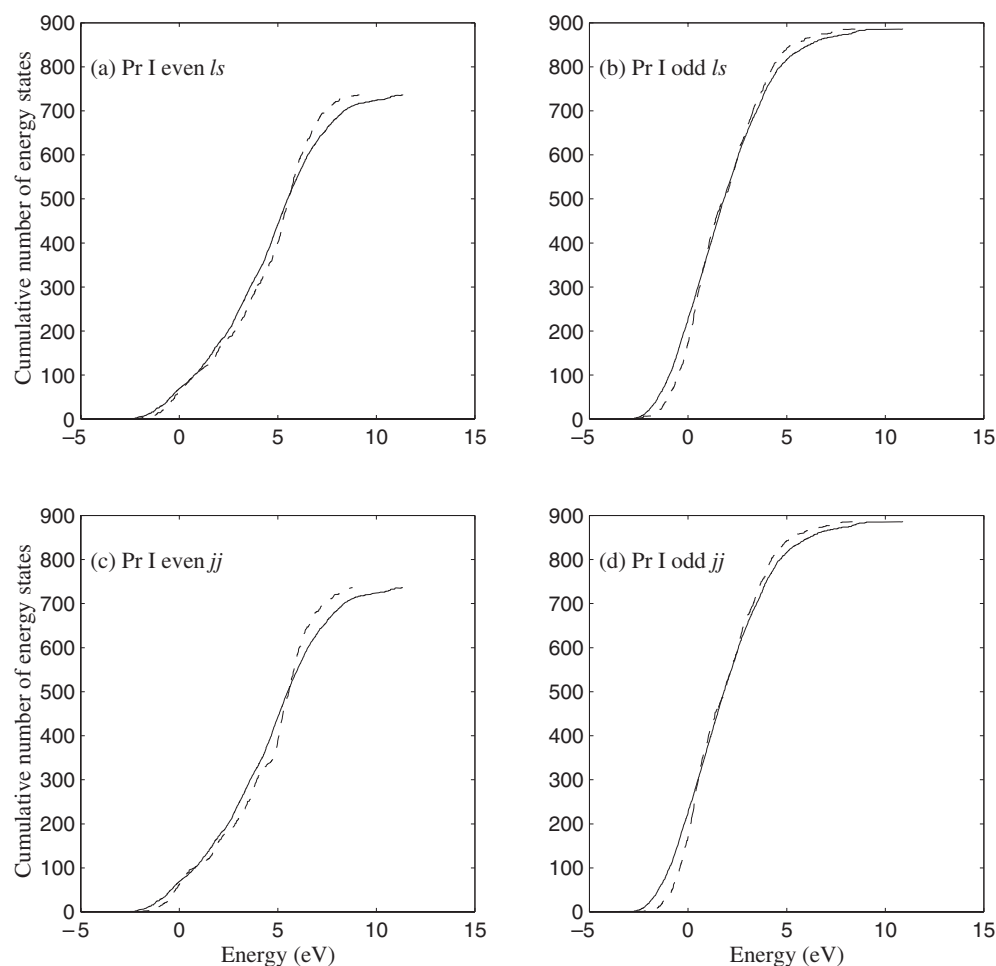
Figure 1. Mode number for the CI (full) and non-CI eigenvalues (broken) of Ce I.

angular momentum, there is a considerable number of 'zero' off-diagonal matrix elements. Configuration interaction (CI) does not destroy the conservation of angular momentum. According to arguments given in [12], one would expect the level density to be closer to a Gaussian shape than to a semi-circle shape. Gaussian-like level densities can be seen in [13] and possibly in odd Pr—see figure 30 of [1]. The transition from Gaussian to semi-circle level density occurs [12, 14, 15] when many-body forces are introduced, lifting the selection rules for interactions between configurations of different angular momentum. The local level density $\rho(E)$ reveals fluctuations of various scales, depending on the range of averaging [12].

3. Level spacing distribution

The effect of CI on the eigenvalues of a system can be seen in figures 1 and 2 for the mode number of Ce and Pr [8]. The broken curves indicate the unperturbed H_0 energy eigenvalues and it can be seen how CI gives rise to level repulsion and a 'straightening' of the cumulative number of energy states. However, the mean level spacing of the eigenvalues is not substantially affected by CI as can be seen in table 2. It can also be seen that D_{eig} (where D is the mean

Figure 2. Mode number for the CI (full) and non-CI eigenvalues (broken) of Pr I.

Table 2. Mean level spacings of the unperturbed levels D and the perturbed levels D_{eig}. Note that D and D_{eig} were calculated for the whole of the energy regions.

	Ce				Pr			
	NIST		Cowan		NIST		Cowan	
	Even	Odd	Even	Odd	Even	Odd	Even	Odd
D (eV)			0.034	0.039			0.015	0.013
D_{eig} (eV)	0.022	0.065	0.034	0.036	0.035	0.084	0.019	0.015

level spacing) is approximately two times smaller for Pr than Ce and therefore Pr has roughly double the average level density. The NIST values shown are, apart from even Ce, factors of two to five greater than the respective Cowan values, which indicates a much greater level density for the Cowan results. This suggests that there are many missing energy values in the NIST data.
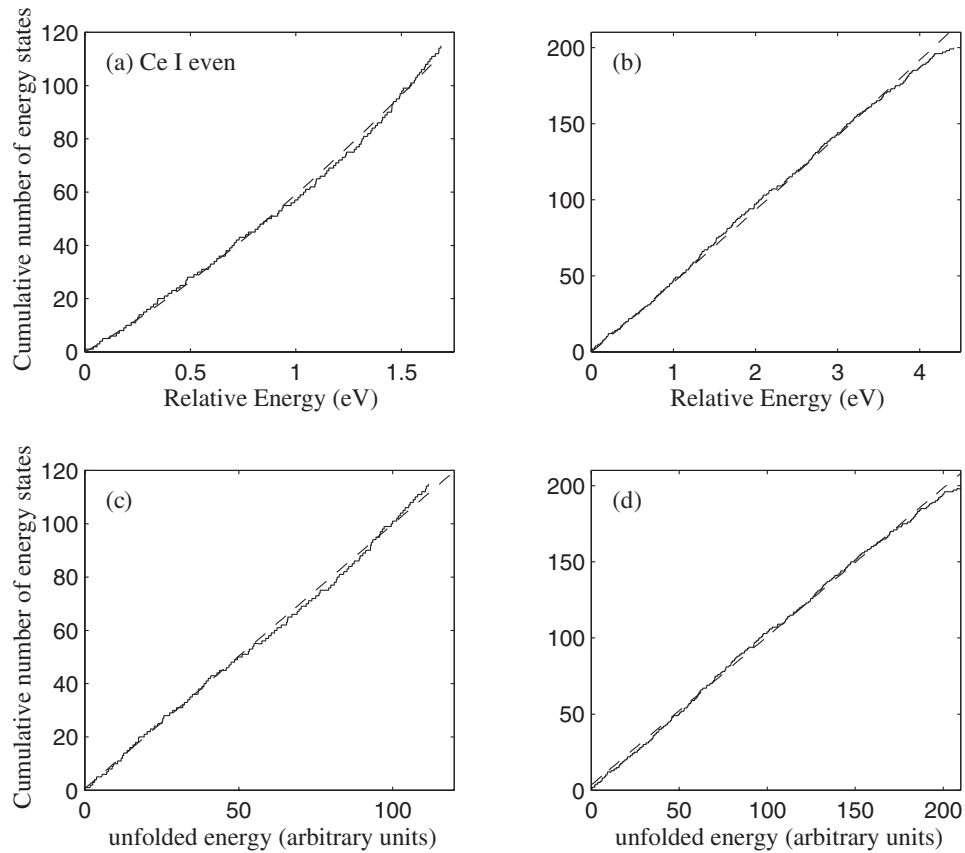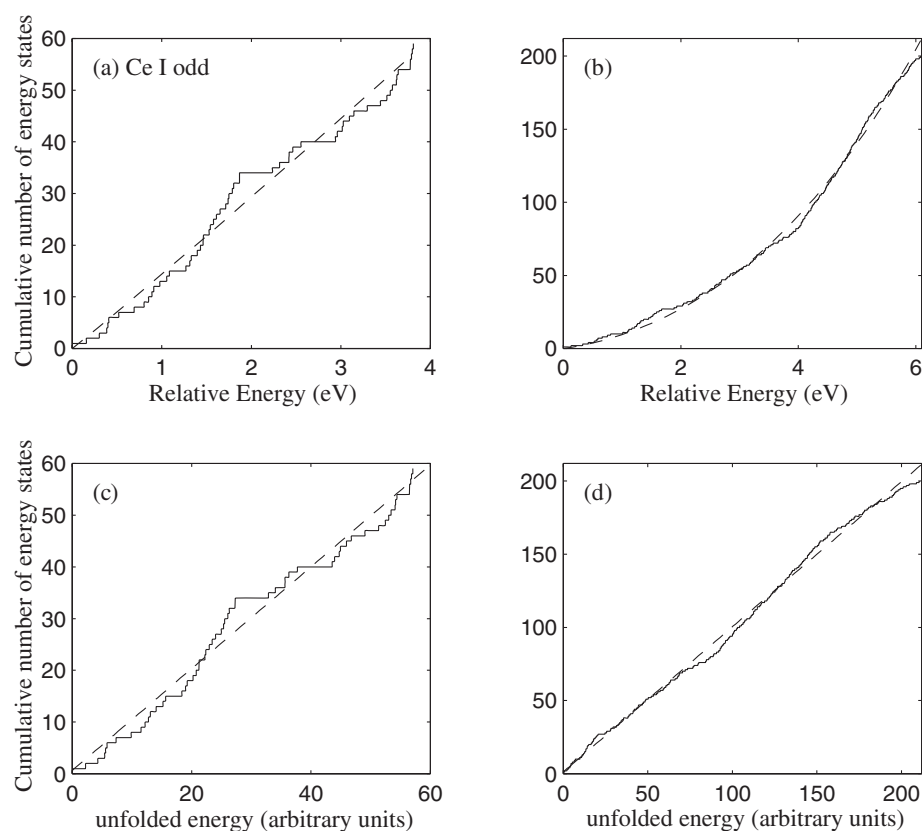
Figure 3. The mode number (full curve) and mean mode number (broken curve) of even Ce. The left column used the experimental values (NIST) [7], whereas the right column used the theoretical values calculated with the HFCI suite of codes [8]. The mode number and mean mode number of the unfolded energy eigenvalues are also shown.

In [13] the effect of CI and non-CI on the nearest neighbour spacing (NNS) of Sm IX was highlighted. It was found that CI gave rise to a Wigner NNS distribution, whereas the non-CI gave rise to a Poisson distribution. In fact, due to intra-CI, i.e. interaction between terms of a configuration, there is disagreement with the Poisson distribution as $s \rightarrow 0$, where s is the nearest neighbour spacing of the unfolded energies.

Before studying the various level statistics, the eigenvalues were unfolded (re-scaled) [16] using the following function for $\overline{N}$, the mean mode number:

$$\overline{N}(\rho_0, a, E) = \int_0^E \rho_0 e^{a\sqrt{E}} \, dE \qquad (1)$$

where ρ_0 and a are treated as curve fitting parameters. Figures 3–6 show the mode number N and the mean mode number $\overline{N}$, for even and odd Ce and Pr. The experimental values of even and odd Pr and also odd Ce show a large number of apparent energy 'gaps'. This is probably due to incomplete data values. However, even Ce appears to have a much smoother appearance for N. The plots of N versus the unfolded energies, which have slopes of m and intercept c, are also shown in figures 3–6. The least squares slope m and intercept c are tabulated along with ρ_0 and a in tables 4 and 5. m is very close to 1.0 for both Ce and Pr and this gives an

Figure 4. The mode number (full curve) and mean mode number (broken curve) of odd Ce.

Table 3. Energy regions (eV) that are unfolded.

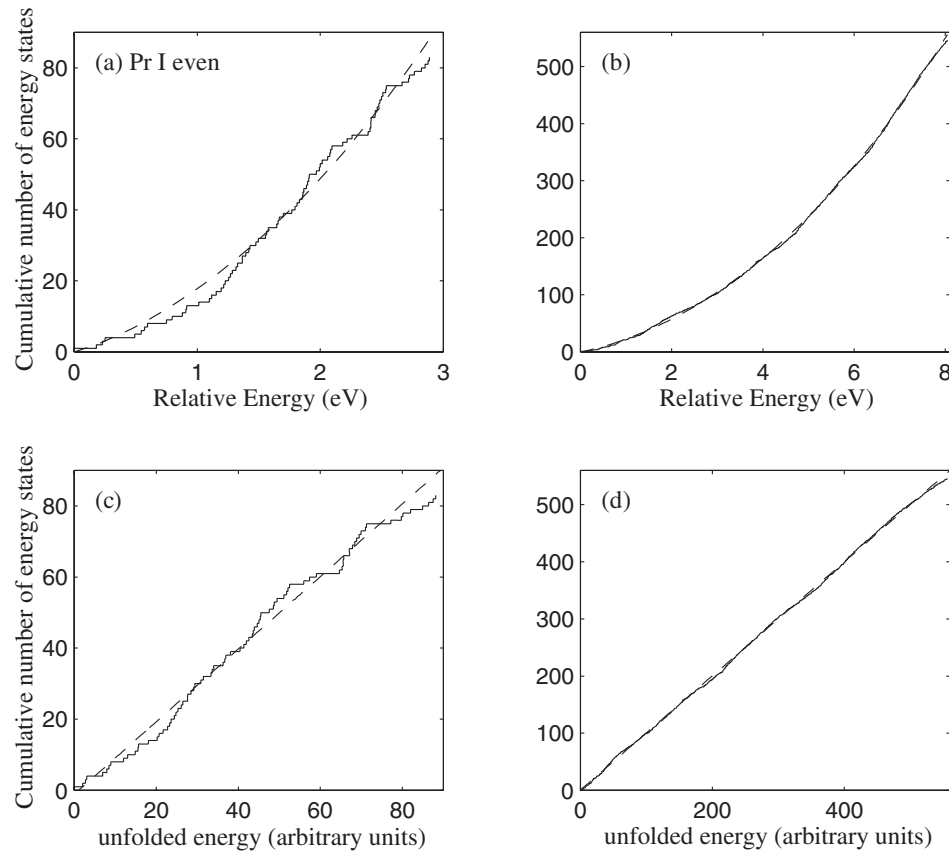|	NIST		Cowan	
	Even	Odd	Even	Odd
Ce	1.91–3.60	0–3.81	−1.39–3.09	0.90–5.19
Pr	0.60–3.49	2.26–3.50	−2.05–5.98	−1.99–1.41

average level density (global) of 1.0 for the unfolded energies. Note that the curve fitting was only calculated for the energy regions shown in table 3. The selected energy regions were also 'zeroed' before the curve fitting procedure.

Using the unfolded energies, the NNS distributions were calculated and are shown in figures 7–10. The Wigner and Poisson distributions are shown as the broken and chain curves, respectively, and represent the extremes of classical behaviour, i.e. regular (Poisson) and 'chaotic' (Wigner). However, in reality, a system usually has a mixture of both regular and chaotic characteristics and the Brody distribution [4, 17, 18] is used to account for this:

$$P(x, \omega) = \alpha(\omega) \cdot (\omega + 1) \cdot x^{\omega} \cdot e^{-\alpha(\omega) \cdot x^{\omega+1}} \tag{2}$$

where $\alpha(\omega) = \Gamma\left(\frac{\omega+2}{\omega+1}\right)^{\omega+1}$.

This is analogous to very few atomic systems having exactly either ls or jj coupling but having an intermediate coupling representation.

Figure 5. The mode number (full curve) and mean mode number (broken curve) of even Pr.

Table 4. Various curve fitting parameters of the energy eigenvalue statistics of Ce I.
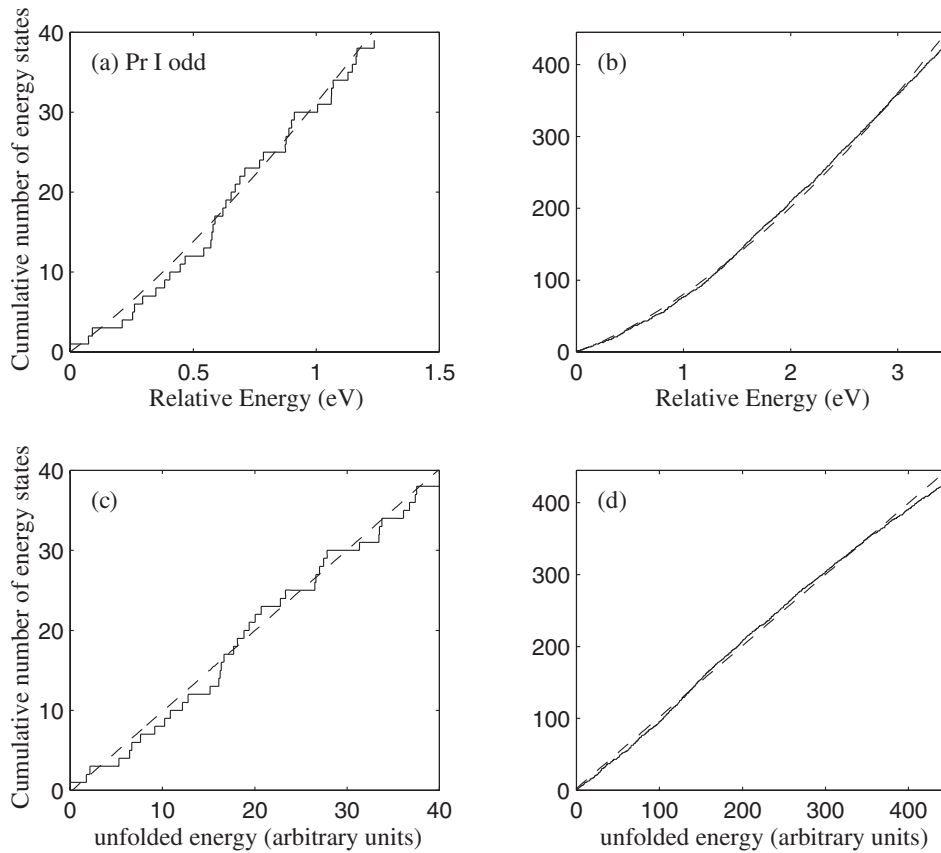
	NIST		Cowan	
	Even	Odd	Even	Odd
ρ_0 (eV^{-1})	40.92	13.80	43.57	4.26
a (eV$^{-1/2}$)	0.54	0.06	0.07	1.15
m	0.99	0.98	0.97	0.99
c	0.65	0.60	3.51	1.21
$1 + \omega$	1.73	1.12	1.65	1.76
% error on $1 + \omega$	2.47	2.72	1.18	3.83
ω	0.73	0.12	0.65	0.76
Covariance of spacings	−0.21	0.06	−0.10	-7×10^{-4}

In order to obtain the Brody parameter ω, a graph of $\ln(\ln[(1 - \Pi(s))^{-1}])$ versus $\ln(s)$ is plotted and ω is found from its slope of $(1 + \omega)$ [19], where $\Pi(s)$ is the cumulative spacing distribution, i.e.

$$\Pi(s) = \int_0^s P(x)\,dx \equiv 1 - e^{-\alpha(\omega) \cdot s^{\omega+1}}. \tag{3}$$

Figures 7–10 show $\Pi(s)$ and $\ln(\ln[(1 - \Pi(s))^{-1}])$ versus $\ln(s)$. The resulting $(1 + \omega)$, and

Figure 6. The mode number (full curve) and mean mode number (broken curve) of odd Pr.

Table 5. Various curve fitting parameters of the energy eigenvalue statistics of Pr I.

	NIST		Cowan	
	Even	Odd	Even	Odd
ρ_0 (eV^{-1})	8.56	20.78	12.85	47.36
a (eV$^{-1/2}$)	1.05	0.59	0.82	0.77
m	1.02	1.01	0.99	0.99
c	−1.17	−0.23	0.35	2.46
$1 + \omega$	1.24	1.02	1.95	1.84
% error on $1 + \omega$	2.77	2.87	1.96	1.70
ω	0.24	0.02	0.95	0.84
Covariance of spacings	0.06	−0.14	−0.11	−0.15

hence ω, are given in tables 4 and 5. The values of ω for the experimental eigenvalues indicate behaviour very close to Poissonian ($\omega = 0$) for even and odd Pr and odd Ce. Even Ce has a value of 0.73 and therefore has more Wigner-like level repulsion ($\omega = 1$). The theoretical ω values of Pr, however, are much closer to the Wigner extreme and in fact it is the even and odd Ce which have the lowest values of ω and this is indicative of intermediate level statistics.
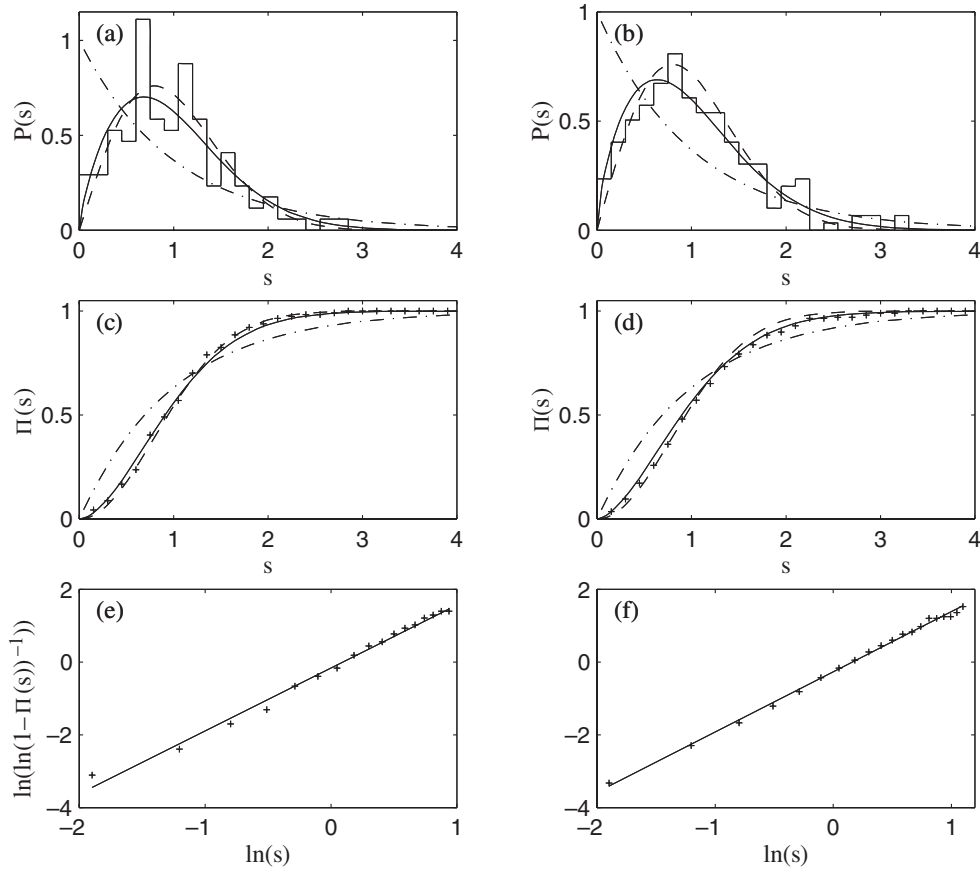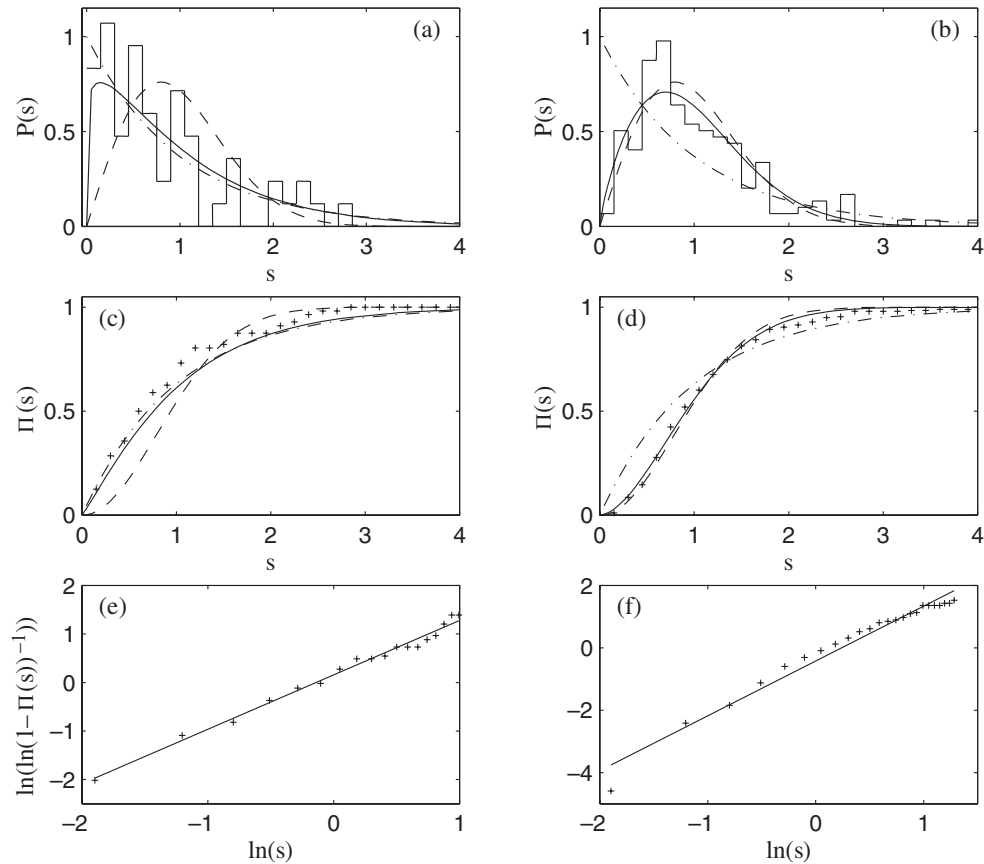
Figure 7. $P(s)$, $\Pi(s)$ and $\ln(\ln(1 - \Pi(s))^{-1})$ for even Ce. The left column used the experimental values (NIST) [7], whereas the right column used the theoretical values calculated with the HFCI suite of codes [8].

Another test for possible GOE behaviour is the covariance of adjacent spacings:

$$\mathrm{cov}(s_n, s_{n+1}) = \frac{\sum_{n=1}^{N} (s_n - \langle s_n \rangle)(s_{n+1} - \langle s_{n+1} \rangle)}{\left[\left(\sum_{n=1}^{N} (s_n - \langle s_n \rangle)^2\right)\left(\sum_{n=1}^{N} (s_{n+1} - \langle s_{n+1} \rangle)^2\right)\right]^{1/2}}. \tag{4}$$

This is sensitive to correlations between levels E_i and E_{i+2} (s is measured on the unfolded energy scale) and is predicted by GOE theory to have the value -0.27 [20]. From tables 4 and 5 it would appear that, for the experimental values, even Ce with a value of -0.21 is the closest to GOE predictions, while odd Ce and even Pr have values that are very close to the Poisson value of 0, i.e. no correlations. It should be noted that the value for odd Pr of -0.14 does not correspond to an ω of almost 0 (Poisson) and is suggestive of more intermediate statistics. ω for the theoretical values of even and odd Pr and even Ce are in correspondence with an ω of intermediate behaviour. However, the value ω of 0.76 and a covariance of approximately 0 for odd Ce is suggestive of an uncorrelated Wigner spectrum [21], i.e. level repulsion but with no correlation between E_i and E_{i+2}.

Figure 8. $P(s)$, $\Pi(s)$ and $\ln(\ln(1 - \Pi(s))^{-1})$ for odd Ce. The left column used the experimental values (NIST) [7], whereas the right column used the theoretical values calculated with the HFCI suite of codes [8].

4. Spectral rigidity

The spectral rigidity $\Delta_3(L)$ [22] is used to distinguish classically chaotic behaviour from regular behaviour in the semi-classical limit. $\Delta_3(L)$ is defined for the interval $[a, a + L]$ in the sequence $\{x_i\}$ as

$$\Delta_3(a, L) = \frac{1}{L} \min_{A,B} \int_a^{a+L} [n(x) - (Ax + B)]^2 \, dx \tag{5}$$

where $n(x)$ is the cumulative number of 'states' of the sequence $\{x_i\}$. For regular dynamics and therefore a random level sequence with the Poisson nearest level spacing distribution, the deviation (i.e. $\Delta_3(L)$) grows linearly, $\Delta_3(L) = L/15$. For the chaotic case and Wigner level spacing distribution the spectra are rigid. Starting at small L with the same linear behaviour as in the regular case, the deviation only grows logarithmically at $L \gg 1$, i.e. $\Delta_3(L) = \frac{1}{\pi^2} \left(\ln(2\pi L) + \gamma - \frac{5}{4} - \frac{\pi^2}{8} \right)$ where this is the GOE spectral rigidity and γ is Euler's constant.

The spectral rigidity [23, 24] results are shown in figures 11–14. The $\langle \rangle$ indicates spectral averaging. It can be seen that, for the NIST data values, only even Ce shows a rigid like
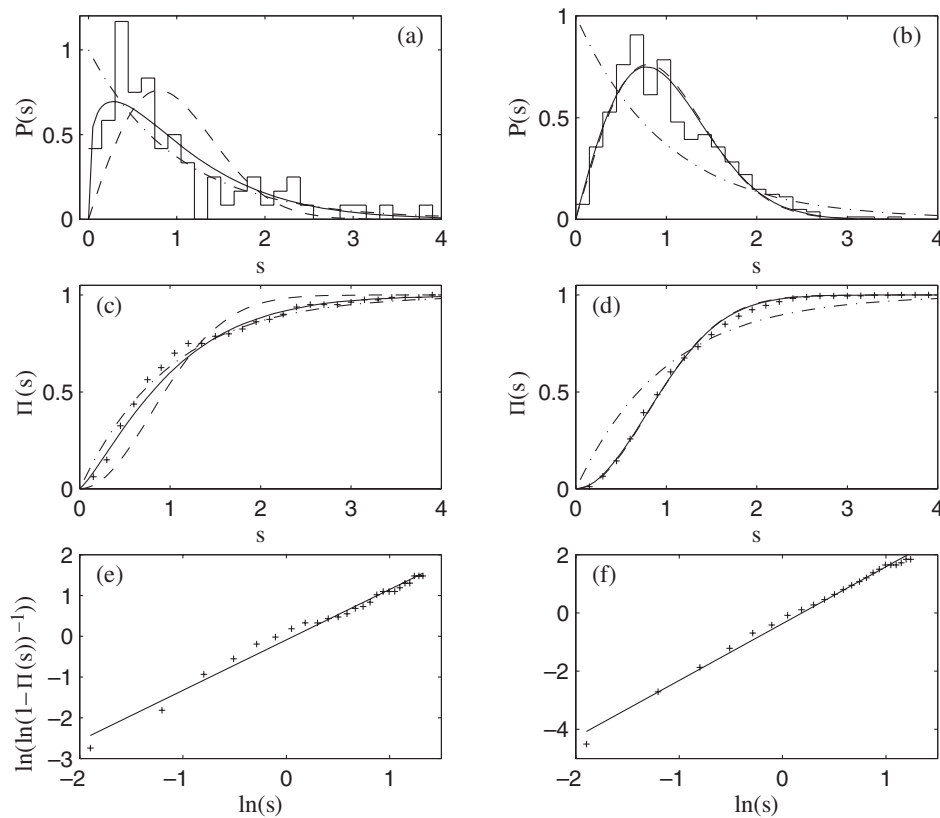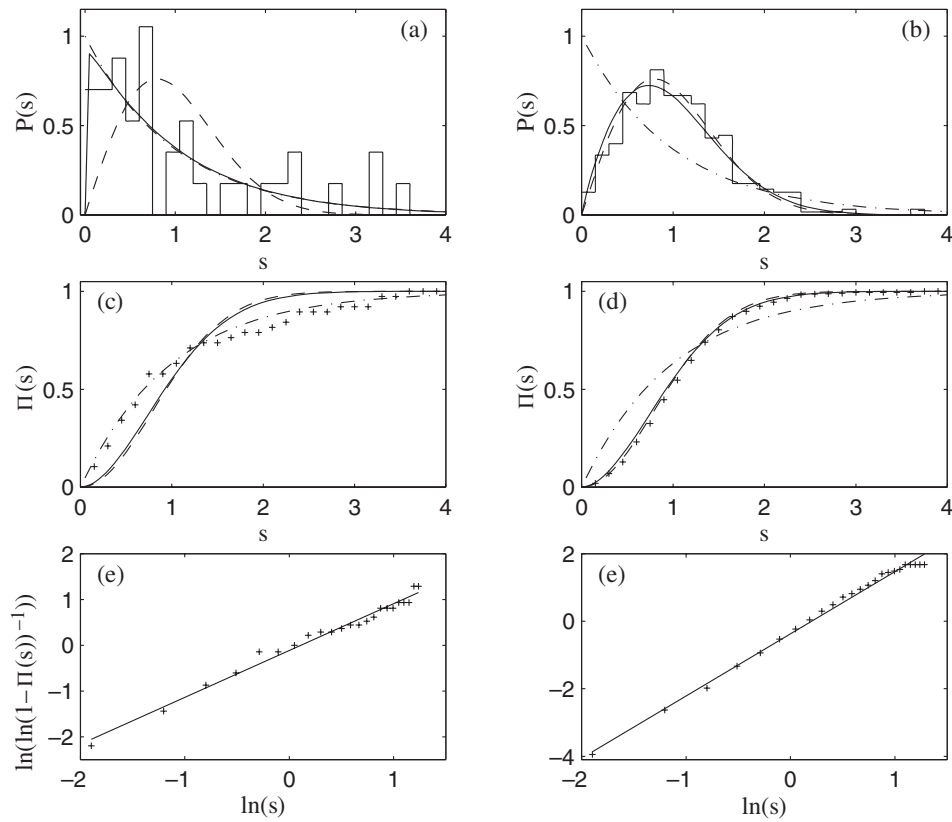
Figure 9. $P(s)$, $\Pi(s)$ and $\ln(\ln(1 - \Pi(s))^{-1})$ for even Pr. The left column used the experimental values (NIST) [7], whereas the right column used the theoretical values calculated with the HFCI suite of codes [8].

spectrum while odd Ce, even Pr and odd Pr follow the Poisson prediction for a limited range of L. Even Ce shows GOE-like behaviour for $L \leqslant 30$ (universal behaviour due to long time periodic orbits [25]) after which the rigidity gradually decreases. For odd Ce and even Pr their spectra follow the Poisson function for $L \leqslant 10\text{--}20$ and then they become apparently less rigid than even the Poisson prediction. Note that for odd Pr $\langle \Delta_3(L) \rangle$ appears to saturate for $L \geqslant 25$, an apparent non-universal result due to short time periodic orbits in the semi-classical regime [25].

For the theoretical results of Cowan, the $\langle \Delta_3(L) \rangle$ for Ce show GOE behaviour for L ranging only from 5 to 10. The even Ce follows the uncorrelated Wigner prediction to $L \approx 130$, after which the spectral rigidity shows an upbend. For odd Ce, the uncorrelated Wigner $\langle \Delta_3(L) \rangle$ is followed until $L \approx 50$, after which the spectral rigidity increases quite dramatically. Even and odd Pr follow the GOE function up to $L \leqslant 20$, after which the $\langle \Delta_3(L) \rangle$ tends towards the uncorrelated Wigner result for $L \leqslant 100$ for even Pr and $L \leqslant 200$ for odd Pr. $\langle \Delta_3(L) \rangle$ in both cases then continues to increase quite rapidly, i.e. becoming less rigid. Note that the $\Delta_3(L)$ for an uncorrelated Wigner spectrum was found to be numerically equal to $\Delta_3(L) = L/[55 - (210/L)]$ for $L > 15$ [21].

All of the Cowan $\langle \Delta_3(L) \rangle$ show intermediate behaviour between Poisson and GOE. This is suggestive, classically, of a mixed phase space of 'regular and chaotic motion'.

Figure 10. $P(s)$, $\Pi(s)$ and $\ln(\ln(1 - \Pi(s))^{-1})$ for odd Pr. The left column used the experimental values (NIST) [7], whereas the right column used the theoretical values calculated with the HFCI suite of codes [8].

5. The correlation-hole method

The correlation-hole method was developed by Leviandier *et al* [26] for the analysis of long range correlations. The properly smoothed Fourier transform $C(t)$ of the spectral autocorrelation function maps the long range correlations onto scales in Fourier space, i.e. $C(t)$ can be written as the Fourier transform of the autocorrelation function of a spectrum $I(x)$ on the unfolded scale x [5]:

$$C(t) = \int_{-\infty}^{+\infty} A(r)e^{2\pi i r t} \, dr \tag{6}$$

where $A(r) = \int_{-\infty}^{+\infty} I(R - r/2)I(R + r/2) \, dR$ is the autocorrelation function of $I(x)$. In the case of a 'stick' spectrum of equal amplitudes $S(E) = \sum_i \delta(E - E_i)$ then [27]

$$|C(t)|^2 = \left| \sum_{j,k} e^{2\pi i (E_j - E_k)t} \right|^2. \tag{7}$$

According to [27] the ensemble average can be simulated by applying a smoothing procedure to the experimental decay function $|C(t)|^2$. It turns out [27] that the most appropriate procedure is a convolution of $|C(t)|^2$ with a Gaussian. Hence, one has to compare the smoothed result
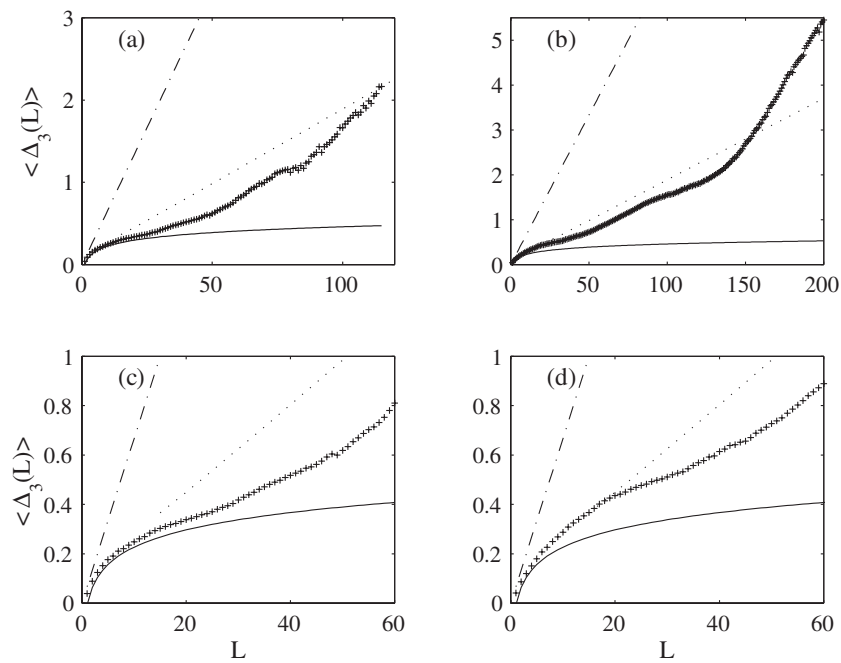
Figure 11. The spectral rigidity of even Ce. Results are shown for Poisson (chain), GOE (full) and uncorrelated GOE (dotted). The left column used the experimental values (NIST) [7], whereas the right column used the theoretical values calculated with the HFCI suite of codes [8].
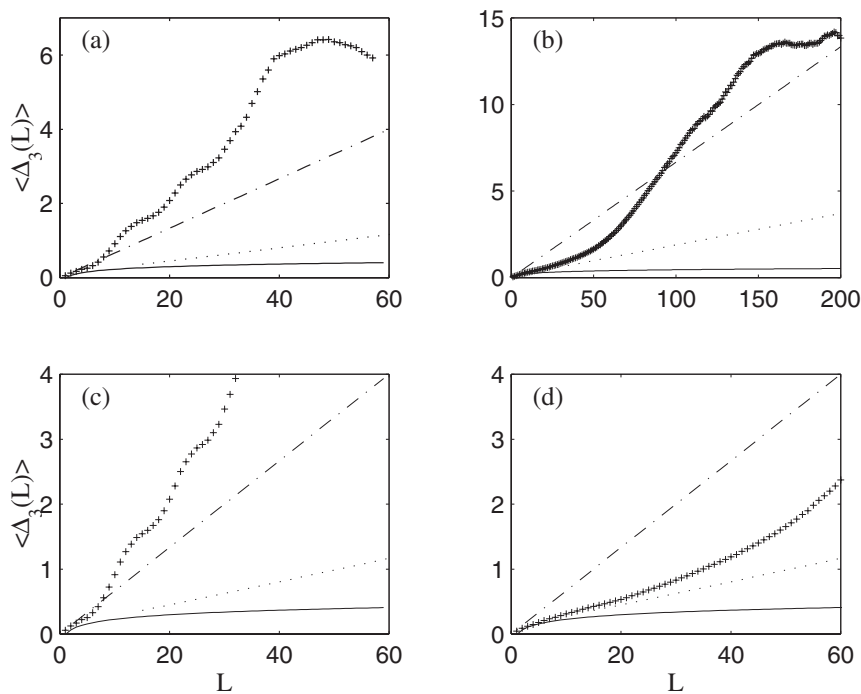
Figure 12. The spectral rigidity of odd Ce. The left column used the experimental values (NIST) [7], whereas the right column used the theoretical values calculated with the HFCI suite of codes [8].
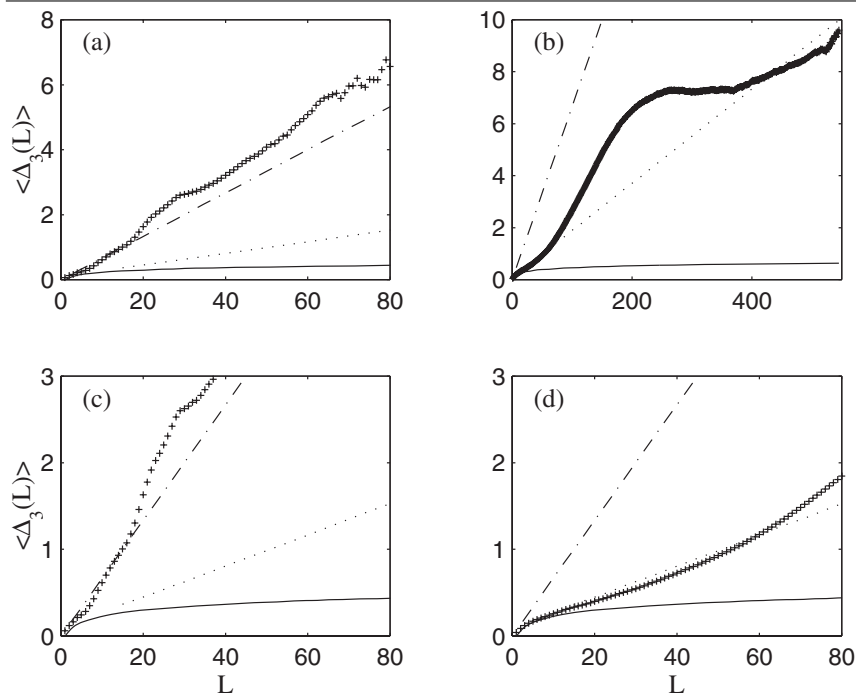
Figure 13. The spectral rigidity of even Pr. The left column used the experimental values (NIST) [7], whereas the right column used the theoretical values calculated with the HFCI suite of codes [8].
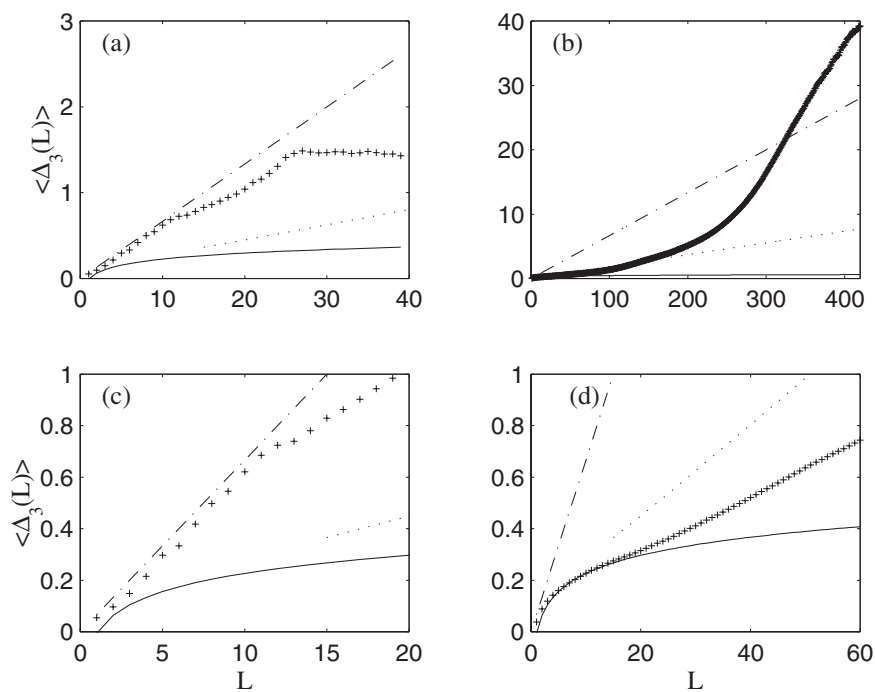
Figure 14. The spectral rigidity of odd Pr. The left column used the experimental values (NIST) [7], whereas the right column used the theoretical values calculated with the HFCI suite of codes [8].

to the function

$$\langle |C(t)|^2 \rangle = \int_{-\infty}^{+\infty} |C(t')|^2 \frac{1}{\sqrt{2\pi\sigma_t^2}} \exp\left(\frac{-(t-t')^2}{2\sigma_t^2}\right) dt' \qquad (8)$$

where the variance was chosen to depend on time as $\sigma_t = t/5$. This procedure is referred to as 'full Gaussian smoothing'. Note that small t in $|C(t)|^2$ corresponds to long range energy correlations in $\Delta_3(L)$. The theoretical $\langle |C(t)|^2 \rangle$ is given by [27]

$$\langle |C(t)|^2 \rangle = N^2 \left(\frac{\sin(\pi N t)}{\pi N t}\right)^2 + N - N b_2(t) \qquad (9)$$

where $b_2(t)$ is the two-level form factor [3, 5] and N is the number of levels in the spectrum. $b_2(t)$ for the GOE is given by

$$b(t) = \begin{cases} (1 - 2t) + t\ln(1 + 2t) & \text{for } t \leqslant 1 \\ -1 + t\ln\left(\dfrac{2t+1}{2t-1}\right) & \text{for } t > 1. \end{cases} \qquad (10)$$

As compared to fluctuations of regular systems, chaotic dynamics causes a considerable suppression of this Fourier transform near the origin, a so-called 'correlation hole'. This has been experimentally observed in the spectra of the molecules acetylene, methylgloxal and nitrogendioxyl [26, 27]. In [26, 28] the nuclear data ensemble was re-analysed and it was shown that nuclear spectra exhibit the correlation hole. For cases intermediate between fully chaotic and regular systems, the correlation hole is less deep and/or abrupt. In particular, a Poisson spectrum should show no correlation hole.

The | Fourier transform |^2 [26, 27], $|C(t)|^2$, of the NIST and Cowan unfolded energies are shown in figures 15–18. Note that the theoretical $\langle |C(t)|^2 \rangle$ shown in the figures was also Gaussian smoothed. It can be seen that all of the Cowan Gaussian smoothed results, $\langle |C(t)|^2 \rangle$, have a clearly visible correlation 'hole' present [26–28]. This can indicate the presence of quantum chaos but false correlation holes can arise even for regular systems [29], for example in uncorrelated Wigner spectra. Note the presence of oscillations on the Cowan $\langle |C(t)|^2 \rangle$. This may be due to finite resolution, i.e. one time channel = 1/number of energy levels, and/or the unfolding procedure associated with missing energy levels [29]. Also, there is no smoothing for $t < 0$ and so this 'asymmetry' is more apparent at t near zero. Apart from even Ce, the NIST $\langle |C(t)|^2 \rangle$ show no correlation hole. This is consistent with the limited Poisson-like behaviour found with the $\langle \Delta_3(L) \rangle$. Note that small t corresponds to large correlation lengths L in $\langle \Delta_3(L) \rangle$ and so the highly oscillatory small time behaviour of $\langle |C(t)|^2 \rangle$ for even and odd Pr and odd Ce shows the effect of non-universal behaviour in the $\langle \Delta_3(L) \rangle$.

Of course all of these results, the NNS, $\langle \Delta_3(L) \rangle$ and $\langle |C(t)|^2 \rangle$, are highly dependent on the unfolding procedure which is greatly affected by missing energy levels. Also, apparent GOE type behaviour can be mimicked if the curve fitting procedure for unfolding is 'too good', resulting in spurious correlations between energy levels.

It should be noted that the study of the nearest neighbour level spacing distribution and $\Delta_3(L)$ with the experimental spectra of Nd, Sm and Tb [20] showed close agreement with the predictions of GOE. This has perhaps relevance to [30], where these elements apparently give rise to $f(\alpha)$ spectra. However, it should be stressed that relatively few energy eigenvalues were used in the $f(\alpha)$ analysis and the levels were not sorted according to parity or J value. Also, note that $\Delta_3(L)$ was calculated in [20] only for L = number of energy eigenvalues and not, as in the present case, for $L \leqslant$ number of energy eigenvalues.

The lack of many-body electron correlations in the Cowan code may give rise to uncorrelated behaviour in $\langle \Delta_3(L) \rangle$ which could lead to a false correlation hole. Also note that in [31] the conclusion was reached that the limited resolution of spectra can influence all of the various level statistics—the NNS, $\langle \Delta_3(L) \rangle$ and $|C(t)|^2$.
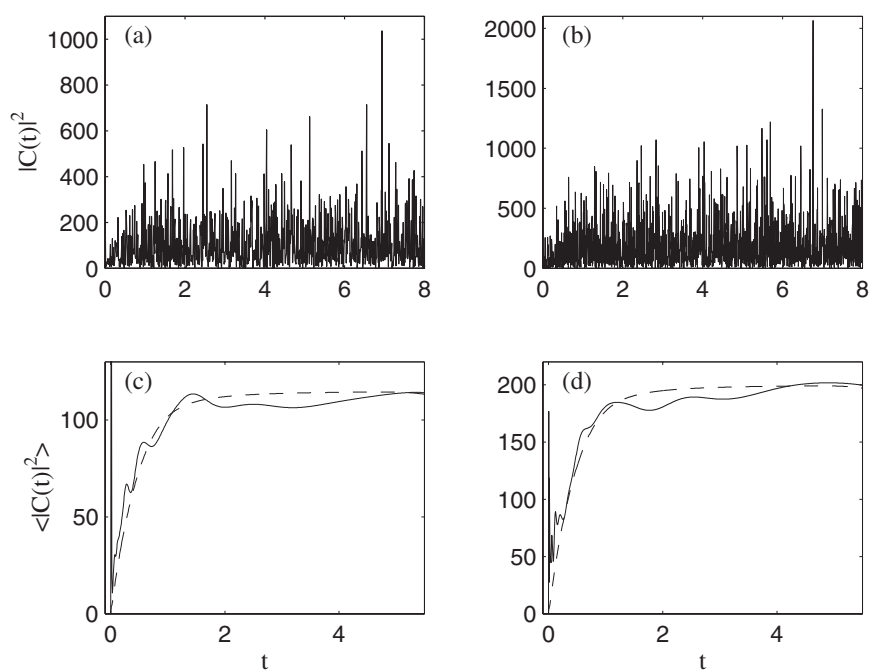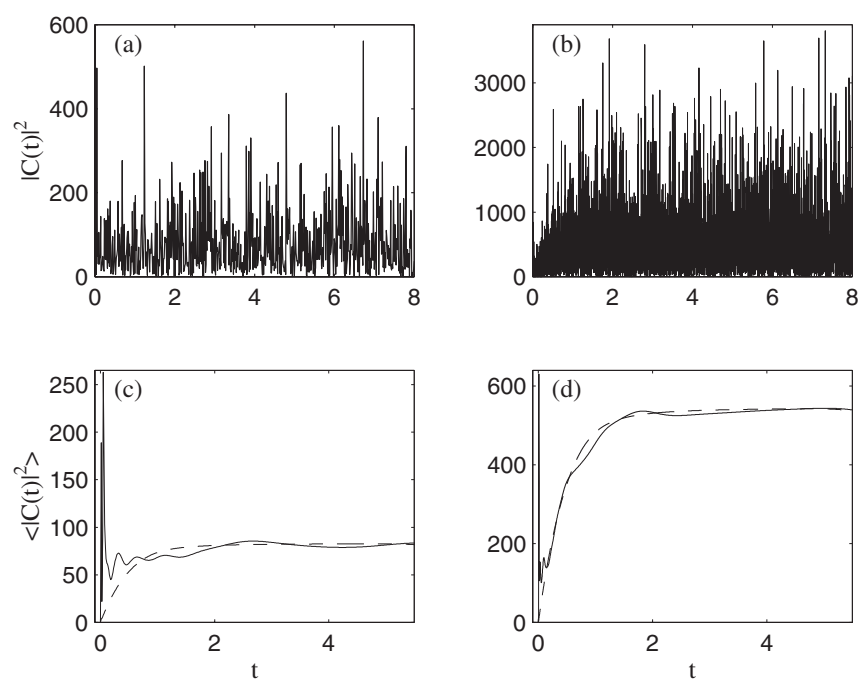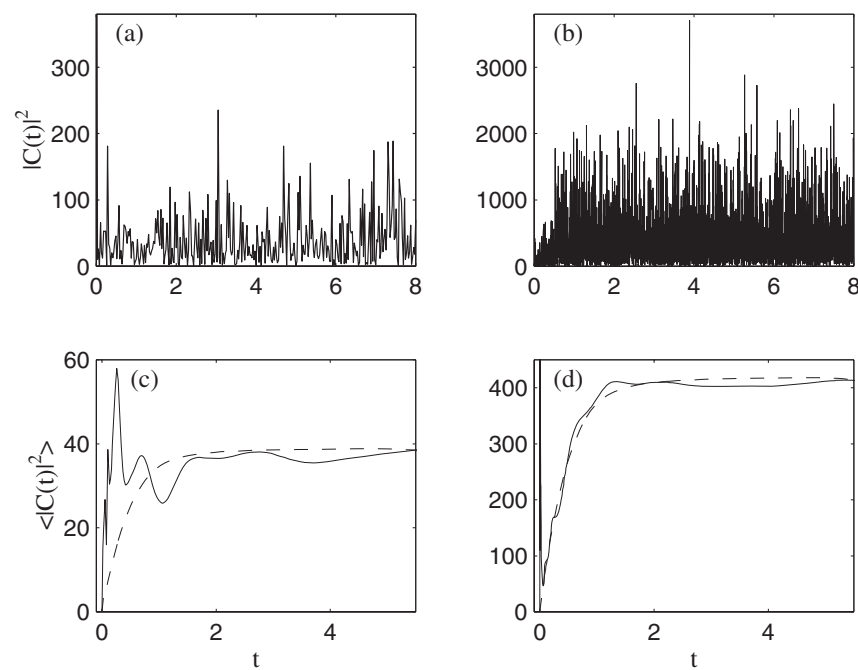
Figure 15. $|C(t)|^2$ and the spectral averaged $\langle|C(t)|^2\rangle$ of the unfolded energies of even Ce. The left column used the experimental values (NIST) [7], whereas the right column used the theoretical values calculated with the HFCI suite of codes [8].
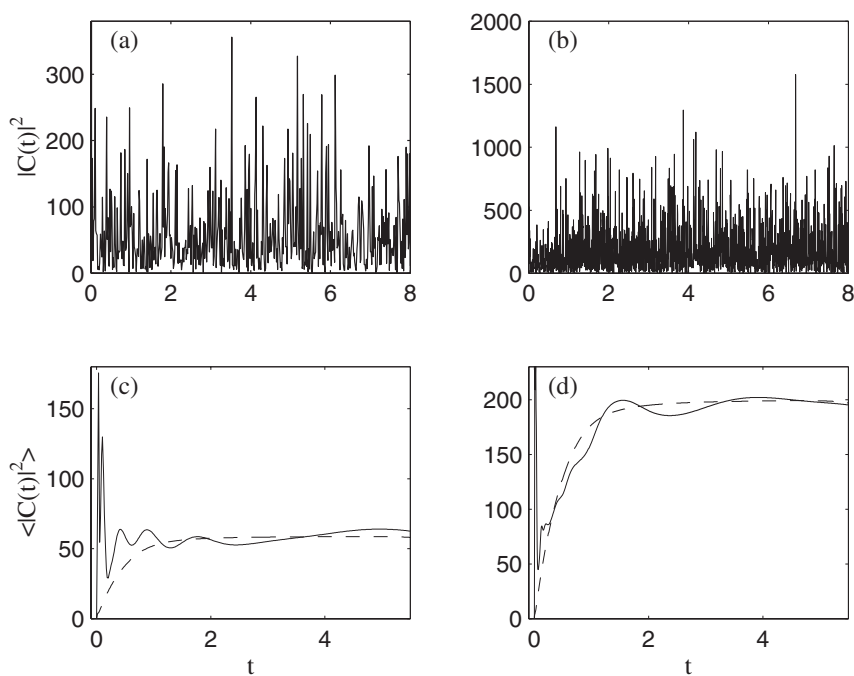
Figure 16. $|C(t)|^2$ and the spectral averaged $\langle|C(t)|^2\rangle$ of the unfolded energies of odd Ce. The left column used the experimental values (NIST) [7], whereas the right column used the theoretical values calculated with the HFCI suite of codes [8].

Figure 17. $|C(t)|^2$ and the spectral averaged $\langle|C(t)|^2\rangle$ of the unfolded energies of even Pr. The left column used the experimental values (NIST) [7], whereas the right column used the theoretical values calculated with the HFCI suite of codes [8].
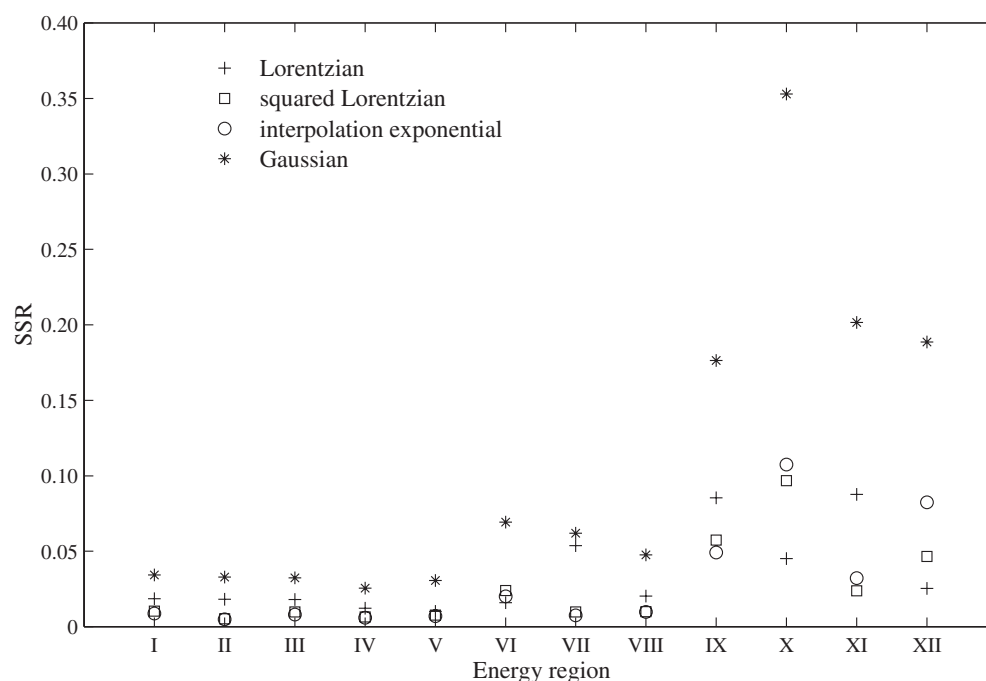

Figure 18. $|C(t)|^2$ and the spectral averaged $\langle|C(t)|^2\rangle$ of the unfolded energies of odd Pr. The left column used the experimental values (NIST) [7], whereas the right column used the theoretical values calculated with the HFCI suite of codes [8].

Figure 19. SSR for the non-normalized $S^{1/2}$ components of Ce.

6. Dipole matrix elements

It is claimed [32] that the dipole matrix elements, $S^{1/2}$, 'will become random (and close to Gaussian) as soon as at least one of the states involved, the initial or the final, moves into the compound-state energy range and becomes a superposition of many random elements'.

To test this proposition, the dipole matrix elements were calculated between even and odd Ce and Pr states (fixed J) and then because the $S^{1/2}$ vary with energy along a spectrum the total spectral region was divided into 0.5 eV sub-regions (note that the energy regions are given relative to zero). As a qualitative guide to the 'goodness of fits', the sums of the squares of the residuals (SSR) were calculated using a non-linear least-squares Marquardt–Levenberg algorithm for the Lorenztian, squared Lorenztian, interpolation exponential and Gaussian distributions. The SSR for the curve fittings are shown in figures 19–22 for various energy regions as indicated in the figure captions. Both non-normalized and normalized $S^{1/2}$ were analysed. The $S^{1/2}$ were normalized by using a running average:

$$S_{ij}^{1/2} = \frac{S_{ij}^{1/2}}{\sqrt{\langle S \rangle}} \tag{11}$$

of ± 6 elements for both Ce and Pr.

Both the non-normalized and normalized $S^{1/2}$ for both Ce and Pr show better quality fits for the squared Lorentzian and interpolation exponential distributions as indicated by the SSR. It can also be seen that, in general, the SSR increase as the energy interval increases, where region I = 0–0.5 eV, region II = 0.5–1.0 eV, etc. Also, for the normalized $S^{1/2}$ components of Ce, regions X to XII have the lowest SSR for the Lorenztian distribution, whereas the opposite is the case for Pr.
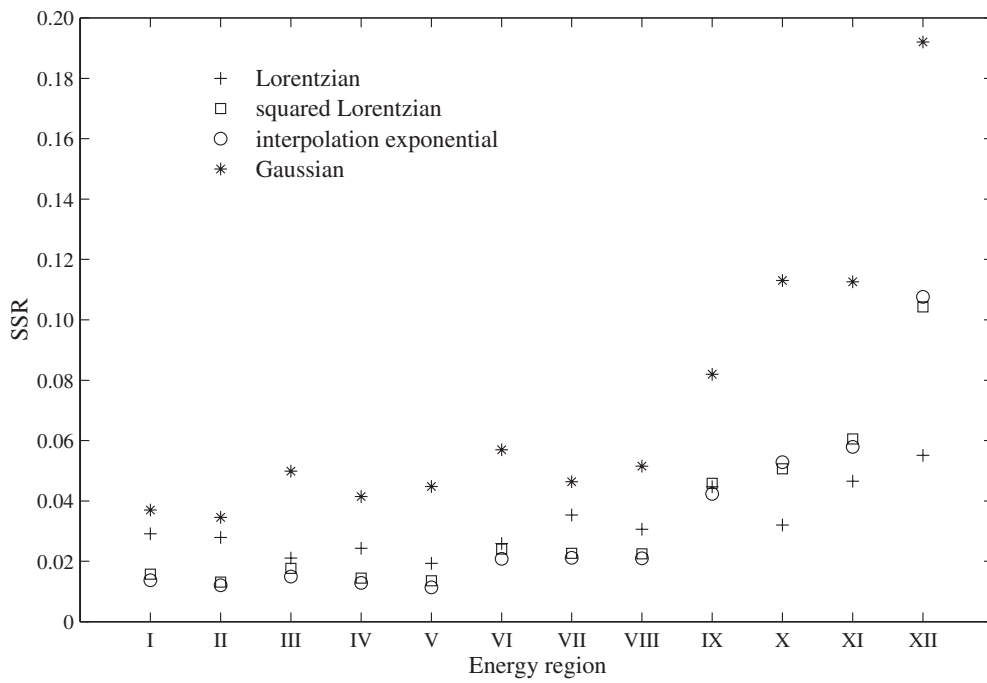
Figure 20. SSR for the normalized $S^{1/2}$ components of Ce.
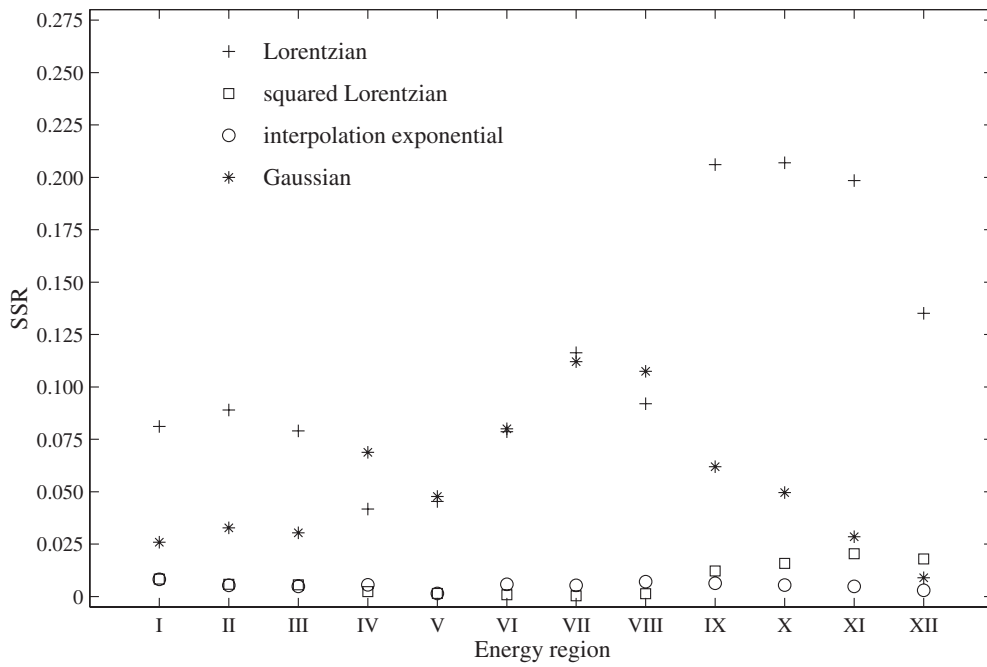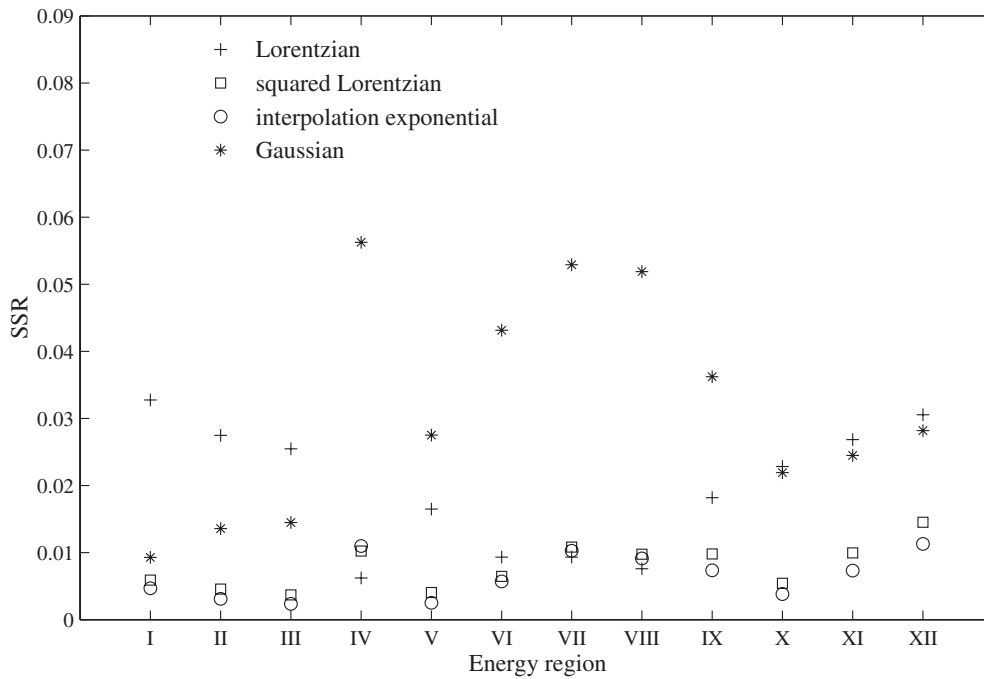
Figure 21. SSR for the non-normalized $S^{1/2}$ components of Pr.

Figure 22. SSR for the normalized $S^{1/2}$ components of Pr.

Examples of the curve fittings for the normalized $S^{1/2}$ are shown in figures 23 and 26, along with their semi-logarithmic companions. From the logarithmic plots it can be observed that the tails (large $|S^{1/2}|$) have, in general, intermediate forms between Lorenztian and Gaussian. A notable exception is that of the normalized $S^{1/2}$ of Ce in region X, where the Lorenztian function is closely followed.

Also, to test the hypothesis at the beginning of this section, the normalized $S^{1/2}$ were squared and the resulting S of the corresponding energy regions were fitted with a χ^2 distribution with a ν degrees fitting parameter. For Gaussian statistics of $S^{1/2}$ a Porter–Thomas distribution with $\nu = 1$ is expected. The $\chi^2(\nu)$ probability distribution is

$$P_{\chi^2}(x; \nu) = \frac{x^{\frac{(\nu-2)}{2}} e^{\frac{-x}{2}}}{2^{\frac{\nu}{2}} \Gamma(\frac{\nu}{2})}. \tag{12}$$

In [33] it was found to be more convenient to use a logarithmic variable as the argument in the $\chi^2(\nu)$ distribution:

$$P_{\chi^2}(\log_{10} x; \nu) = \frac{\ln(10)(\frac{\nu x}{2})^{\frac{\nu}{2}} e^{\frac{-\nu x}{2}}}{\Gamma(\frac{\nu}{2})}. \tag{13}$$

The SSR for the curve fitting to $P_{\chi^2}(\log_{10} S; \nu)$ and the resulting ν are shown in figures 27 and 28 for Ce and Pr respectively. For Ce a ν of ≈ 0.8 is obtained with ν varying from 0.7 to 0.9 for Pr. This suggests that the $S^{1/2}$ are not fully Gaussian and that the corresponding classical system has a mixed phase space [33]. Only for $\nu = 1$ is a fully chaotic system expected. Thus this mixture of many weak and strong lines (i.e. $\nu < 1$) indicates, semi-classically, a mixed phase space consisting of regular (corresponding to integrability and regular classical motion) and irregular states (corresponding to non-integrability and chaos) as postulated by
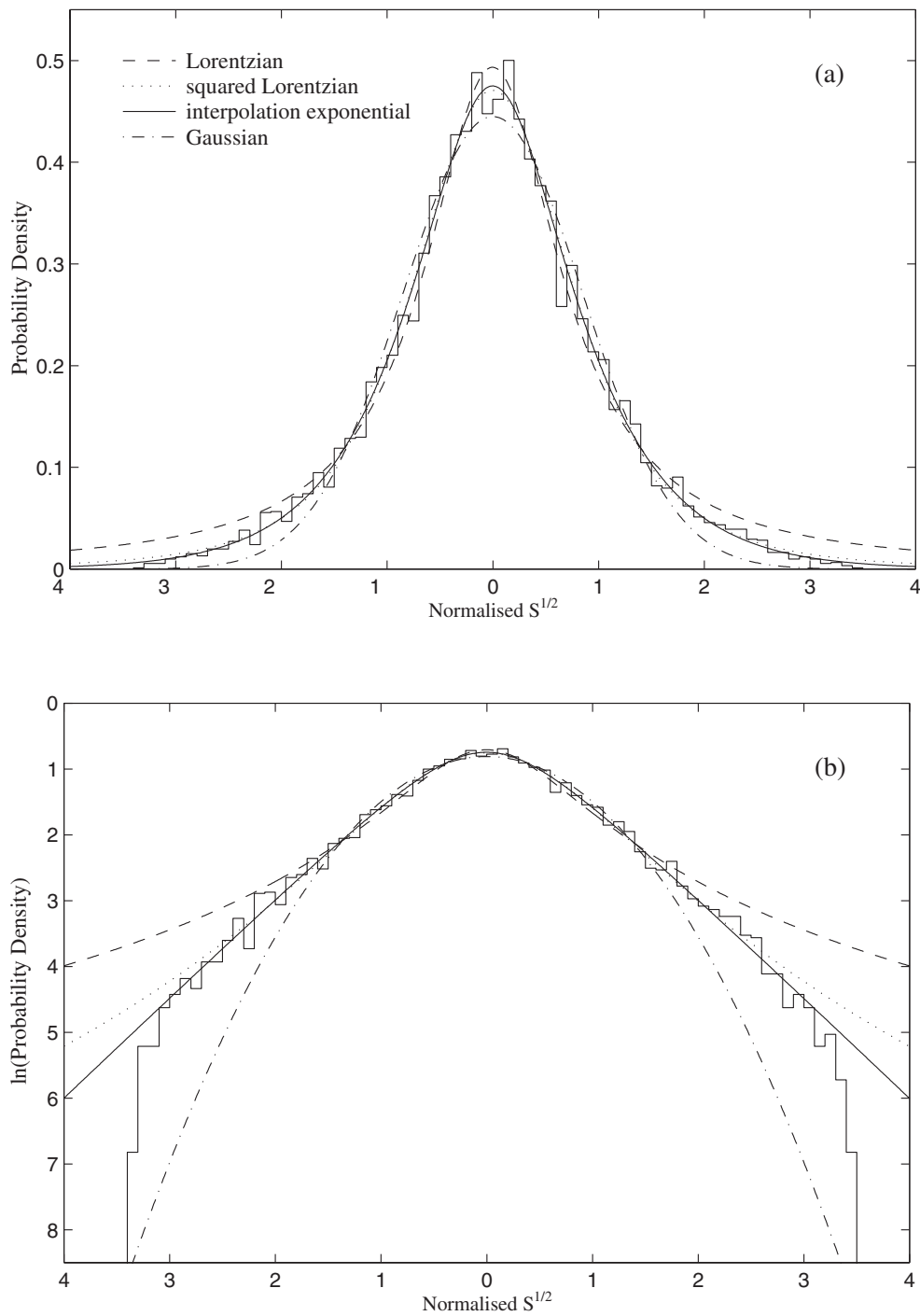
Figure 23. (*a*) The distribution of the normalized $S^{1/2}$ components of Ce and least squares fitting to (i) Lorentzian (broken) (ii) squared Lorenztian (dotted) (iii) interpolation exponential (full) (iv) Gaussian (chain) in energy region II (*b*) The logarithm of the distribution of the normalized $S^{1/2}$ components of Ce in the energy range II.
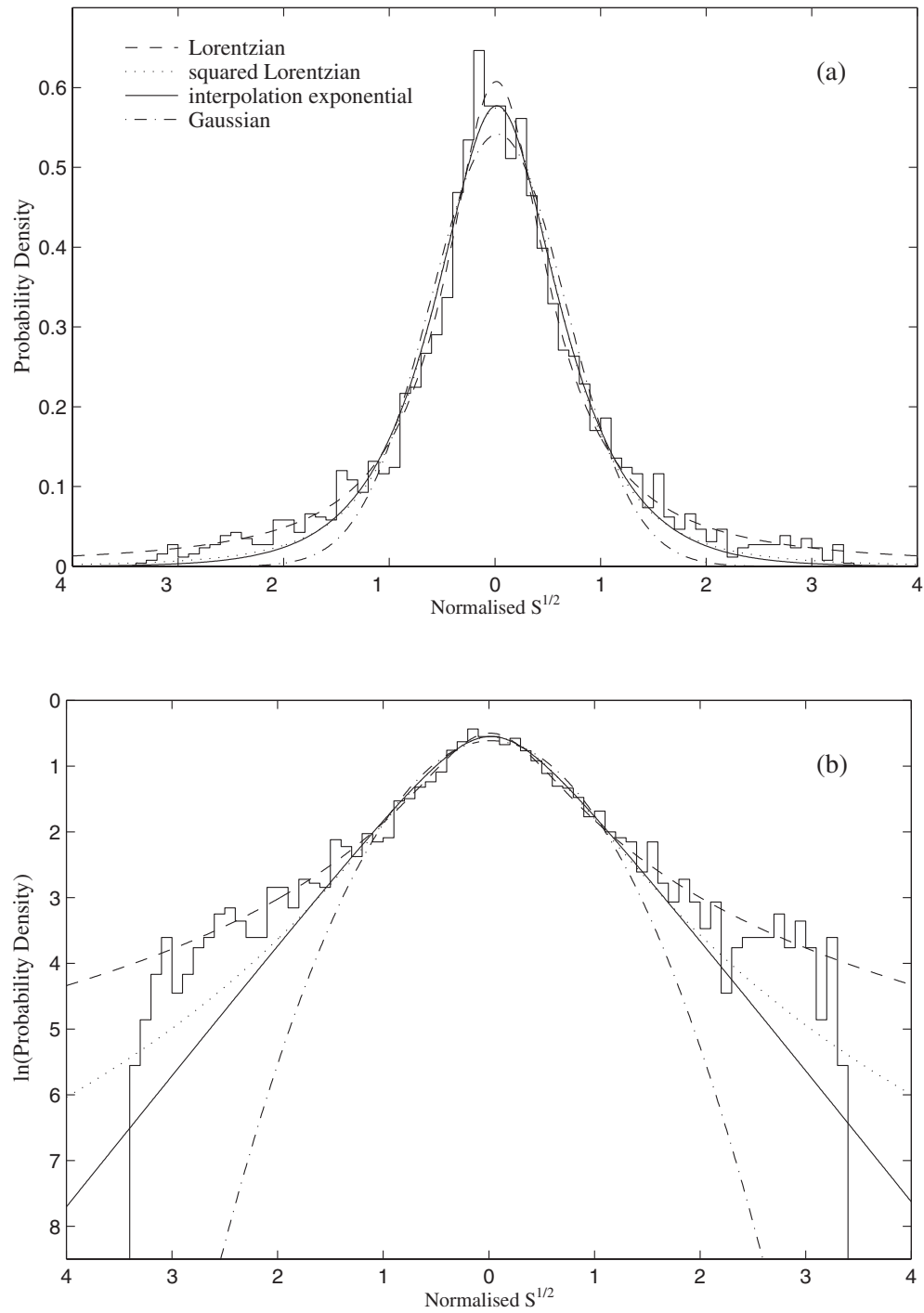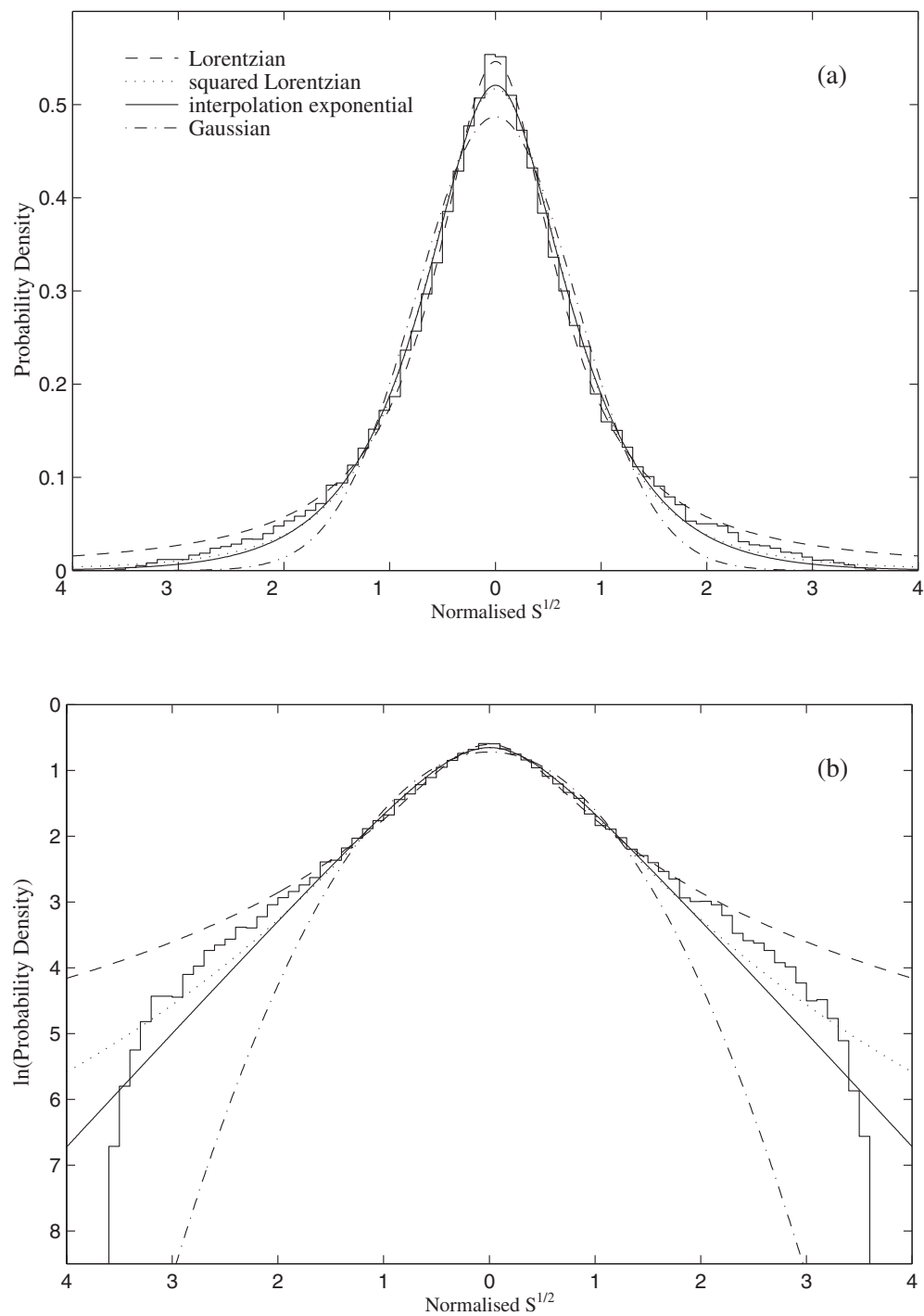
Figure 24. (*a*) The distribution of the normalized $S^{1/2}$ of Ce in the energy range X. (*b*) The logarithm of the distribution of the normalized $S^{1/2}$ components of Ce in the energy range X.
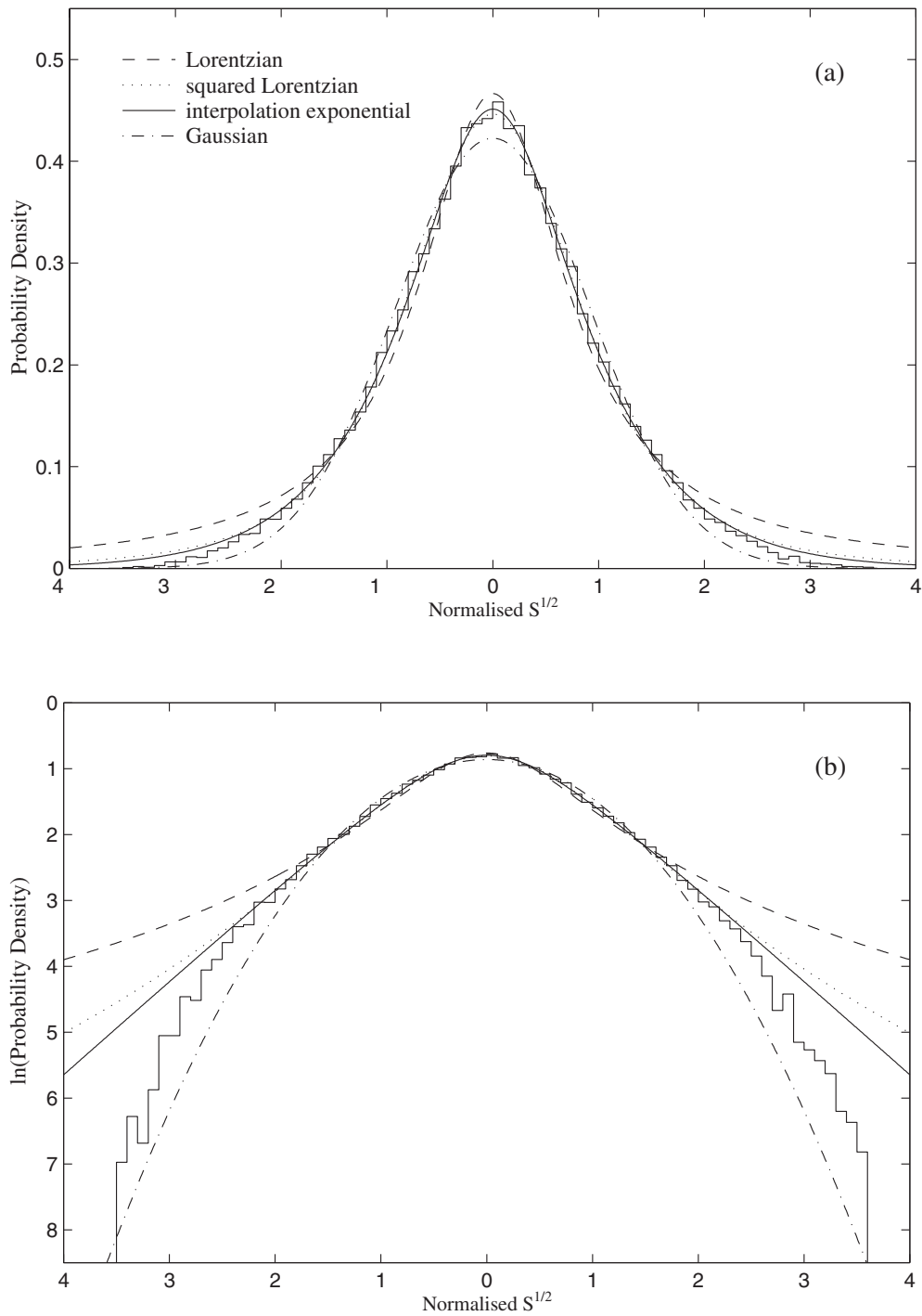
Figure 25. (*a*) The distribution of the normalized $S^{1/2}$ components of Pr in the energy range II. (*b*) The logarithm of the distribution of the normalized $S^{1/2}$ components of Pr in the energy range II.
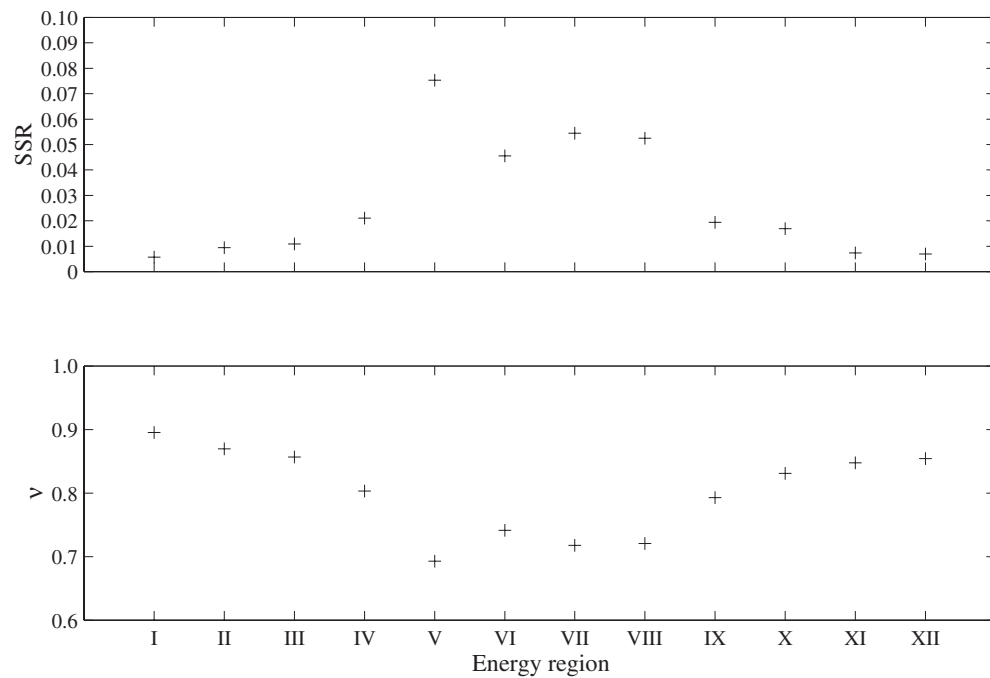
Figure 26. (*a*) The distribution of the normalized $S^{1/2}$ of Pr in the energy range VIII. (*b*) The logarithm of the distribution of the normalized $S^{1/2}$ components of Pr in the energy range VIII.
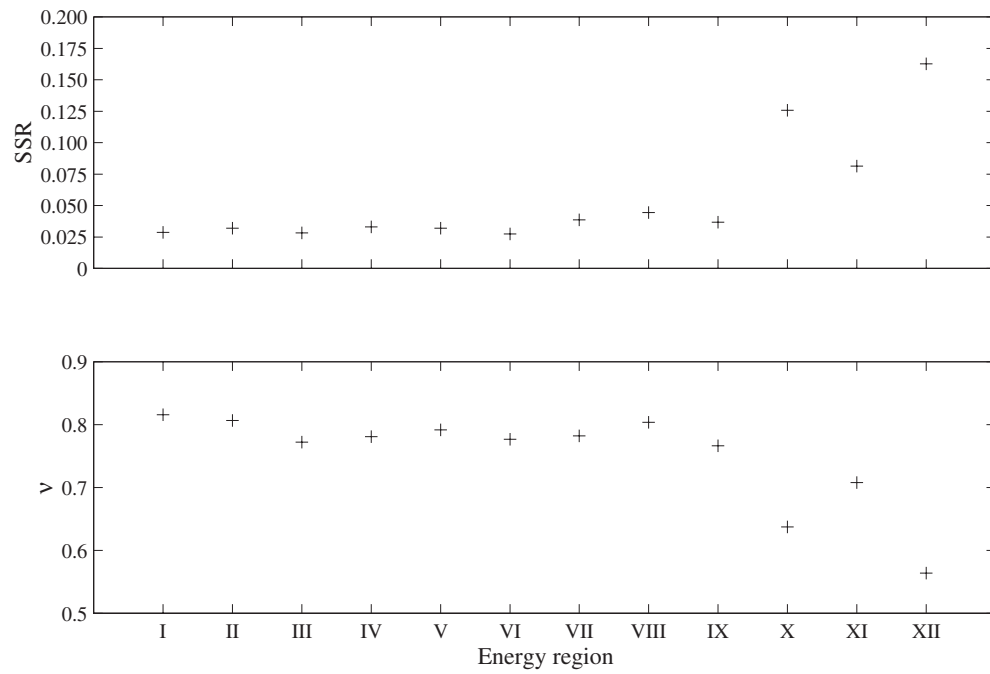
Figure 27. SSR for the normalized S components of Ce to the function $P_{\chi^2}(\log_{10} S; \nu)$.

Figure 28. SSR for the normalized S components of Pr to the function $P_{\chi^2}(\log_{10} S; \nu)$.

Percival [34], with the regular states being highly localized and the irregular states being much more delocalized. Examples of the distributions of the normalized S are shown in figures 29 and 30. However, it must be emphasized that the calculational apparatus of the Cowan code—using the independent particle model, with a mean field, and the corresponding relativistic HFCI equations—and its inherent lack of many-body correlations may contribute significantly to this apparent mixture of regular and irregular states. Note that $S^{1/2}$, and thus S, are basis representation independent and hence are invariant measures, i.e. $S^{1/2}$ is the same in both ls and jj coupling since it is the actual energy eigenvector function(s) that is used to calculate the $S^{1/2}$, and although the composition of the basis states varies from one basis set to another, Ψ, the energy eigenvector does not.

7. Conclusion

It can thus be seen from the results of the present and previous study that one needs a barrage of statistical tests with which to indicate the presence or absence of quantum chaos in an atomic system. It is also found that, because of the basis representation dependence of the Hamiltonian and coupling matrices and the inability of many of the statistics to distinguish very complex behaviour, as would be expected classically for a many-body system, from genuine 'chaotic' behaviour, the invariant measures of level statistics are perhaps the best candidates with which to search for signatures of quantum chaos. However, a complete set of energy eigenvalues is ideally required to reach any definitive conclusion, although the presence of extra levels due to improper energy level assignments can also be a possible source of error. It must be emphasized that the unfolding process is fraught with difficulties that can lead to spurious correlation and/or non-correlation effects. Also, it must be stressed that no one statistic by itself can determine the presence or absence of 'quantum chaos'.

All of the statistical tests indicate intermediate behaviour between regular and 'chaotic' regimes for the Cowan code (HFCI) results. In particular, the line strengths are suggestive, semi-classically, of a mixed phase space of regular and irregular states [34]. However, the level statistics for the NIST data should be viewed as highly tentative, given the restricted number of energy levels.

Although including many more configurations in calculations is highly desirable (in order to give more basis states), one wonders if the resulting statistics are just a product of extreme complexity and have no connection with quantum chaos, i.e. what one ideally requires is a 'simple' atomic system with which to probe the regimes of quantum chaos and where there is no inherent complexity involved 'to begin with'.

Future studies should include the use of 'proper' many-body calculations that have many-body correlation effects included. Other possible atomic systems that are being used to search for signatures of quantum chaos [32] include doubly excited states and inner-shell excitation spectra of alkaline earth atoms or even multiply excited states of light atoms [4, 18, 35]. The inclusion of continuum effects should also be included in future studies.

A possible candidate with which to search for the signatures of quantum chaos is highly ionized Sm [13] and further along the rare-earth sequence. The reason for this surmise is due to the collapse of the 4f radial wavefunction which leads to large off-diagonal matrix elements, $\langle \psi_a | H | \psi_b \rangle$ (of course, this is basis dependent), for many of the matrix elements of the Hamiltonian and also because of the presence of a high level density for the unperturbed levels and hence small unperturbed level spacings. However, [36] have found an additional selection rule in complex rare-earth spectra originating from strong exchange interaction which may be thought of as arising from the presence of a new quantum number. This, classically, represents another 'constant of motion' and suggests that the system cannot attain a fully chaotic
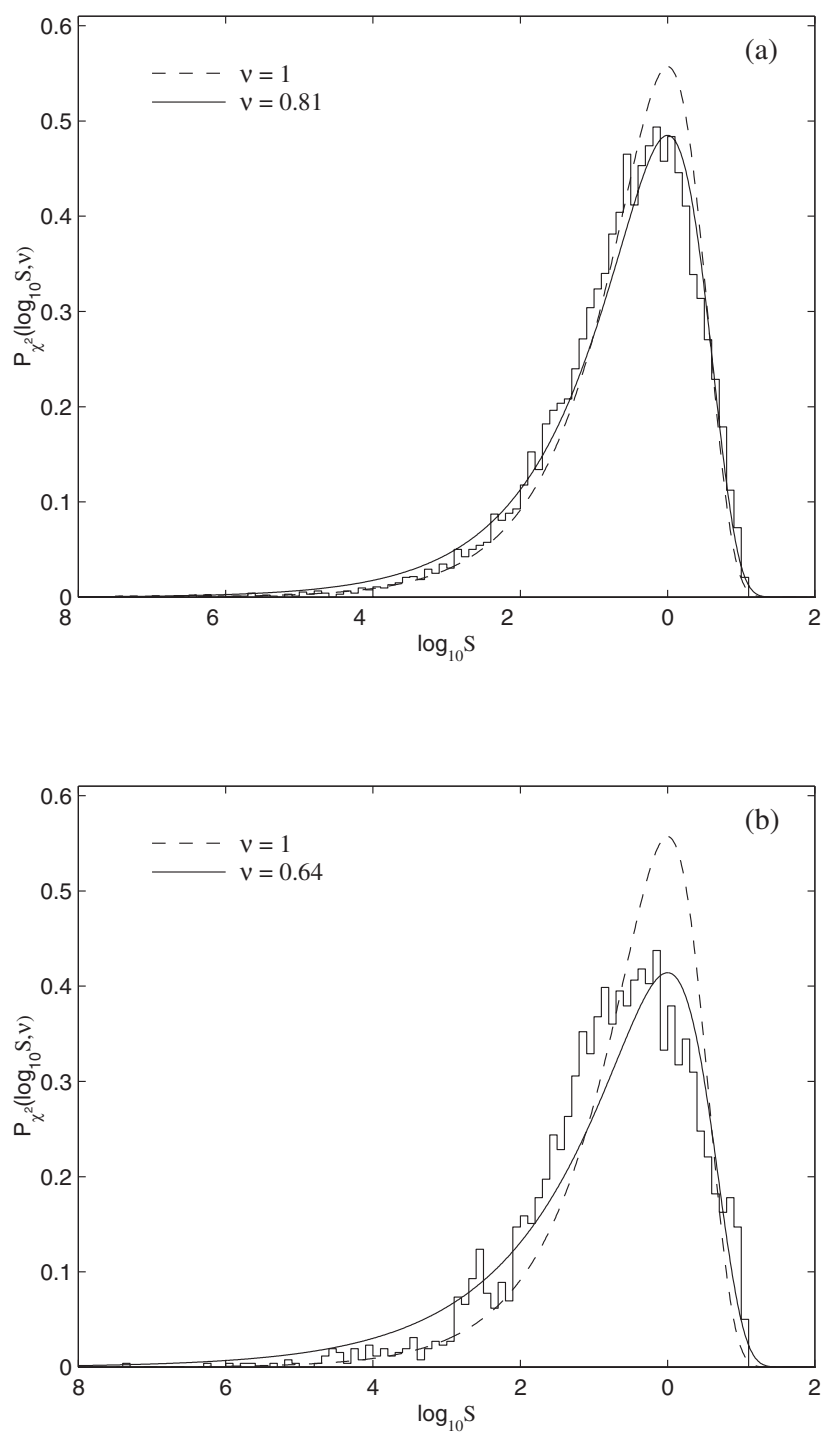
Figure 29. (*a*) The distribution of the normalized *S* components of Ce in energy region II. (*b*) The distribution of the normalized *S* components of Ce in energy region X.
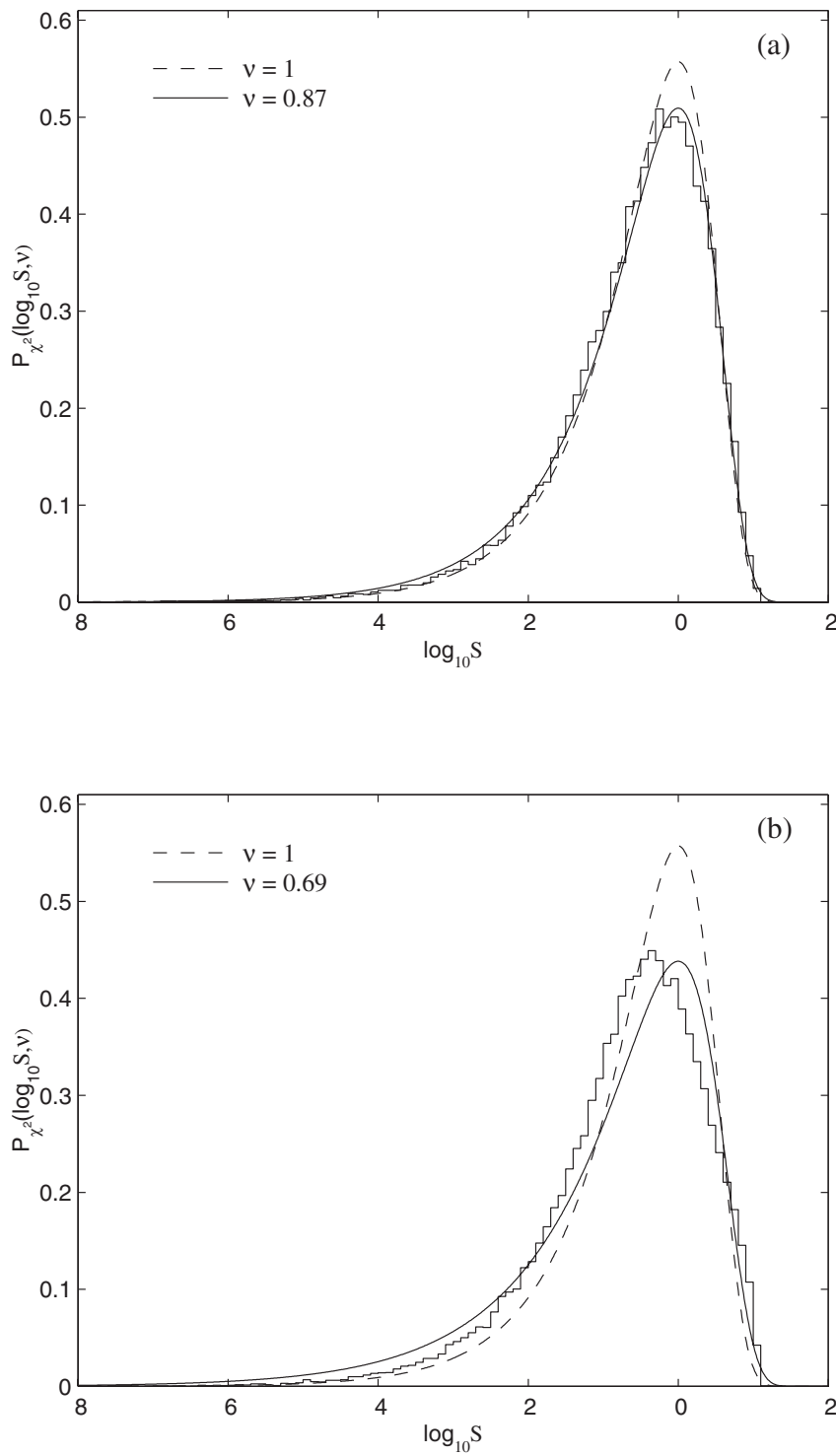
Figure 30. (*a*) The distribution of the normalized *S* components of Pr in energy region II. (*b*) The distribution of the normalized *S* components of Pr in energy region V.

state. In fact, a 'good' quantum number reflects the presence of some type of symmetry. How this additional symmetry would affect the predictions of RMT is an interesting avenue for exploration.

In summary, the cerium atom calculations have not only been performed by methods different from previous studies (thus critically cross-examining the data obtained earlier) but a few finer statistical tests have been added, using for example the spectral rigidity and the correlation-hole method. A broader range of methods is vital in spectroscopic studies where no single method alone is known to provide a decisive test of regular versus chaotic behaviour. The results for the Pr I atom are new and important for extracting universal features common to all (or many) rare-earth atoms and distinguishing them from element-specific characteristics.

Acknowledgments

References

[1] Cummings A, O'Sullivan G and Heffernan D M 2001 Signatures of quantum chaos in rare earth elements: I. Characterization of the Hamiltonian matrices and coupling matrices of Ce I and Pr I using the statistical predictions of Random Matrix Theory *J. Phys. B: At. Mol. Opt. Phys.* **34** 3407
[2] Flambaum V V, Gribakina A A, Gribakin G F and Kozlov M G 1994 *Phys. Rev.* A **50** 267–96
[3] Mehta M L 1991 *Random Matrices, Revised and Enlarged* 2nd edn (New York: Academic)
[4] Connerade J-P 1997 *J. Phys. B: At. Mol. Opt. Phys.* **30** L31–8
[5] Guhr T, Müller-Groeling A and Weidenmüller H A 1998 *Phys. Rep.* **299** 190–245
[6] Bohigas O, Giannoni M J and Schmit C 1984 *Phys. Rev. Lett.* **52** 1
[7] http://physics.nist.gov/cgi-bin/AtData/main_asd
[8] Cowan R D 1981 *The Theory of Atomic Structure and Spectra* (Berkeley, CA: University of California Press)
[9] Casati G, Molinari L and Izrailev F 1990 *Phys. Rev. Lett.* **64** 1851–4
[10] Kús M, Lewenstein M and Haake F 1991 *Phys. Rev.* A **44** 2800
[11] Fyodorov Y V and Mirlin A D 1991 *Phys. Rev. Lett.* **67** 2405
[12] Brody T A, Flores J, French J B, Mello P A and Wong S S M 1981 *Rev. Mod. Phys.* **53** 385
[13] O'Sullivan G, Carroll P K, Dunne P, Faulkner R, McGuinness C and Murphy N 1999 *J. Phys. B: At. Mol. Opt. Phys.* **32** 1893–922
[14] French J B and Wong S S M 1971 *Phys. Lett.* B **35** 5
[15] Mon K K and French J B 1975 *Ann. Phys., NY* **95** 90
[16] Friedich H 1991 *Theoretical Atomic Physics* (Berlin: Springer)
[17] Brody T A 1973 *Lett. Nuovo Cimento* **7** 1482
[18] Connerade J-P, Grant I P, Marketos P and Oberdisse J 1995 *J. Phys. B: At. Mol. Opt. Phys.* **28** 2539–51
[19] Badrinarayanan R and José J V 1995 *Quantum Chaos Between Order and Disorder* ed G Casati and B Chirikov (Cambridge: Cambridge University Press) p 596
[20] Camarda H C and Georgopulos P D 1983 *Phys. Rev. Lett.* **50** 492
[21] Camarda H *et al* 1972 Statistical properties of nuclei *Proc. Int. Conf. on Statistical Properties of Nuclei (Albany, Aug. 1971)* ed J B Garg (New York: Plenum) pp 205–13
[22] Dyson F J and Mehta M L 1963 *J. Math. Phys.* **4** 701
[23] Bohigas O and Giannoni M J 1975 *Ann. Phys., NY* **89** 393
[24] Ormand W E and Broglia R A 1992 *Phys. Rev.* C **46** 5
[25] Berry M V 1985 *Proc. R. Soc.* A **400** 229
[26] Leviander L, Lombardi M, Jost R and Pique J P 1986 *Phys. Rev. Lett.* **56** 2449
[27] Delon A, Jost R and Lombardi M 1991 *J. Chem. Phys.* **95** 5701
[28] Lombardi M, Bohigas O and Seligman T H 1994 *Phys. Lett.* B **324** 263
[29] Lombardi M, Labastie P and Bordas M C 1988 *J. Chem. Phys.* **89** 3479–90

[30] Cummings A, O'Sullivan G, Hanan W G and Heffernan D M 2001 Multifractal analysis of selected rare-earth elements *J. Phys. B: At. Mol. Opt. Phys.* 2547–73
[31] Michaille L and Pique J-P 1999 *Phys. Rev. Lett.* **82** 2083–6
[32] Flambaum V V, Gribakina A A and Gribakin G F 1998 *Phys. Rev.* A **58** 230–7
[33] Adams A A, Mitchell G E and Schriner J F Jr 1998 *Phys. Lett.* B **422** 13–8
[34] Percival I C 1977 Semiclassical theory of bound states *Adv. Chem. Phys.* **36** 1
[35] Connerade J-P, Baig M A and Sweeney M 1990 *J. Phys. B: At. Mol. Opt. Phys.* **23** 713
[36] O'Sullivan G 2000 (Private communication with R Karazija)